Journal of Magnetic Resonance **137,** 413–429 (1999)
Article ID jmre.1998.1693, available online at http://www.idealibrary.com on IDEAL®

Measurement of Magnitude and Sign of Heteronuclear Coupling Constants in Transition Metal Complexes

Gottfried Otting,*[,1] Linnea P. Soler,† and Barbara A. Messerle†

*Department of Medical Biochemistry and Biophysics, Karolinska Institute, S-171 77 Stockholm, Sweden; and
†Department of Organic Chemistry, University of Sydney, Sydney, New South Wales 2006, Australia

Received October 21, 1998; revised December 15, 1998

Sets of specifically tailored E.COSY-type correlation experiments and double-quantum/zero-quantum (DQ/ZQ) experiments are presented which enable the determination of sign and size of small heteronuclear coupling constants across the metal center of transition metal complexes. For the octahedrally coordinated complexes, [Ru(TPM)(H)(CO)(PPh_3)]$^+$[BF_4]$^-$ (1) and [Ir(TPM)(H)(CO)(CO_2CH_3)]$^+$[BF_4]$^-$ (2), 14 of 15 and 15 of 15 possible two-bond scalar coupling constants across the metal center were measured, respectively, using ^{15}N and ^{15}N/^{13}C enriched samples (TPM = tris(1-pyrazolyl)methane)). The reduced coupling constants $^2K_{X\text{-}M\text{-}Y} = 4\pi^2\,{}^2J/(h\gamma_X\gamma_Y)$ were found to be positive when the coupled nuclei X and Y were *trans* with respect to the metal center, and negative when the coupled nuclei were in *cis* position. The validity of this sign rule was verified for J_{CC}, J_{NN}, J_{PN}, J_{PC}, J_{CN}, J_{HP}, J_{HC}, and J_{HN} couplings. Idiosyncracies associated with 2D NMR spectra for the sign determination of coupling constants with ^{15}N which lead to corrections for the signs of J_{HN}, J_{PN}, and J_{CN} couplings reported previously are discussed.

Key Words: **sign of scalar coupling constants; E.COSY-type experiments; DQ/ZQ experiments; long-range correlation experiments.**

INTRODUCTION

NMR provides a powerful tool for the rapid analysis of the stereochemical structure of reactive transition metal complexes. The determination of the relative disposition of ligands about the metal center is central to the determination of the structure of such complexes. Nuclear Overhauser effects are most readily used to elucidate the relative conformation of ligands which contain protons. When the ligands contain heteronuclei with spin 1/2 but few or no protons, scalar coupling constants yield more easily accessible information. For example, stereochemical information is contained in the magnitude of ^2J coupling constants across the metal center as ^2J(*trans*) is usually significantly larger than ^2J(*cis*) for transition metals from the second and third rows of the periodic system (*1–6*). Furthermore, the absolute signs of these scalar coupling constants are dependent on the relative disposition of ligands about the metal center being, as a rule, positive and negative for ^2K(*trans*) and ^2K(*cis*), respectively (*5, 6*). *K* denotes the reduced coupling constant, $K = 4\pi^2J/(h\gamma_I\gamma_S)$, where γ_I and γ_S are the gyromagnetic ratios of the coupling spins and *h* is Planck's constant. While this sign rule seems to hold for transition metal complexes from the second and third rows of the periodic system, reversed relative magnitudes and signs of ^2K(*trans*) and ^2K(*cis*) couplings have been reported for metal centers from the first row of transition metals in the periodic system (*1, 2, 4–7*), a situation which is not further discussed here.

Although the sign rule offers a useful criterion for the geometric disposition of ligands in a metal complex, the experimental base for the sign rule is relatively small (*5, 6*). In the following, the validity of the sign rule is demonstrated for two octahedrally coordinated transition metal complexes, [Ru(TPM)(H)(CO)(PPh_3)]$^+$[BF_4]$^-$ and [Ir(TPM)(H)(CO)(CO_2CH_3)]$^+$[BF_4]$^-$ (Fig. 1), containing ^{1}H, ^{31}P, ^{13}C, and ^{15}N spins in the first coordination sphere. Measurement of all 15 possible ^2J coupling constants between the metal-binding spins was attempted to rule out sign changes due to small deviations from octahedral coordination. Complete sets of improved two-dimensional E.COSY-type and DQ/ZQ experiments are presented which allow the determination of the absolute signs of the coupling constants by relating them to the known sign of a one-bond coupling constant.

In a previous study of a different metal complex containing a Ru ion with ^{15}N and ^{31}P nuclei in an octahedral coordination shell, we concluded that $^2J(trans) > 0$ and $^2J(cis) < 0$ (*8*). This conclusion is shown to be erroneous. Because of the negative gyromagnetic ratio of the ^{15}N nucleus, the ^{15}N frequency axis should be reversed (see the Appendix) (*9*), changing the signs of all J_{HN}, J_{PN}, and J_{CN} coupling constants reported in Refs. (*8*) and (*10*). The signs of all other couplings, in particular those of J_{NN} couplings, were correct.

In the present study, all heteronuclear correlation spectra were plotted in the conventional way, irrespective of the signs of the gyromagnetic ratios of the nuclei involved. Consequently, a positive tilt of an E.COSY-type ^{13}C–^{1}H (^{31}P–^{1}H) cross peak indicates identical signs of J_{CX} (J_{PX}) and J_{HX}, where X denotes a common coupling partner not excited during the

[1] To whom correspondence should be addressed, at: Karolinska Institute, MBB, Doktorsringen 9A, S-171 77 Stockholm, Sweden. Fax: +46-8-315296; e-mail: gottfried.otting@mbb.ki.se.

1090-7807/99 $30.00

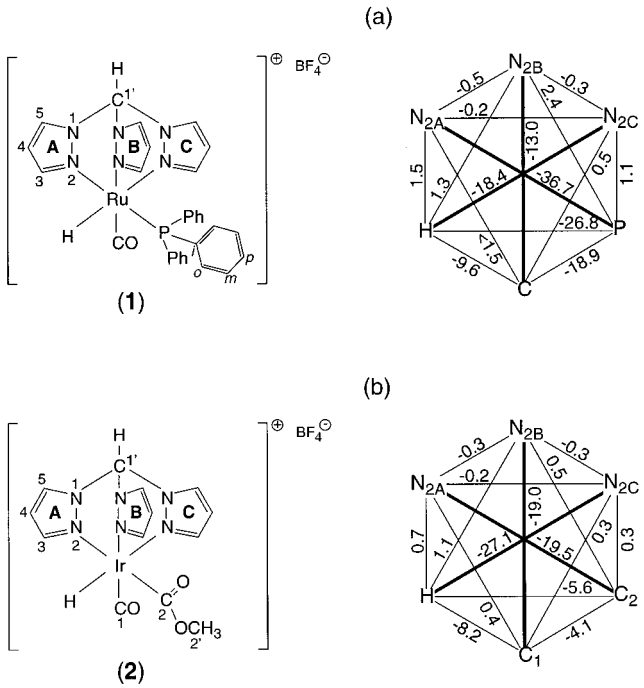

FIG. 1. Chemical structure and coupling constants (in Hz) across the metal center of (a) compound **1,** $[Ru(TPM)(CO)(H)(PPh_3)]^+[BF_4]^-$, and (b) compound **2,** $[Ir(TPM)(H)(CO)(CO_2CH_3)]^+[BF_4]^-$. The magnitudes and absolute signs of the scalar coupling constants are the result of this work.

experiment, whereas a positive tilt in a ^{15}N–^{1}H cross peak indicates different signs of J_{NX} and J_{HX} (see the Appendix).

Many of the experiments were tailored to the coupling constants and chemical shifts encountered in the compounds used here. A comprehensive overview is provided to illustrate the underlying general strategy for the sign determination and to provide a framework for analogous work with other compounds. It is demonstrated that sign and size of coupling constants less than 0.5 Hz can readily be measured.

CHEMICAL SYNTHESIS

*[Ru(TPM)(H)(CO)(PPh$_3$)]$^+$[BF$_4$]$^-$ (**1**)*

An equimolar solution of 99% ^{15}N labeled TPM (54 mg) (*10*) and $[RuH(CO)Cl(PPh_3)_3]$ (237 mg) (*11*) in toluene (30 ml) was degassed via three freeze/pump/thaw cycles and placed under an atmosphere of N_2. The solution was refluxed vigorously for 3 h and subsequently allowed to cool. The toluene was removed under reduced pressure. A solution of $NaBF_4$ (40 mg) in methanol (25 ml) was added. $[Ru(^{15}N\text{-}TPM)(CO)(H)(PPh_3)]^+[BF_4]^-$ (**1**) precipitated while the reaction mixture was stirred for 3 h and was isolated as a pale grey powder (80 mg, 47%).

*[Ir(TPM)(H)(CO)(CO$_2$CH$_3$)]$^+$[BF$_4$]$^-$ (**2**)*

Compound **2,** $[Ir(TPM)(H)(CO)(CO_2CH_3)]^+[BF_4]^-$, was prepared using a modification of the procedure described by Oro *et al.* (*12*). Ninety-nine percent ^{15}N labeled TPM (48 mg, 0.22 mmol), $[Ir(1.5\text{-cyclooctadiene})Cl]_2$ (714 mg, 0.106 mmol), and $NaBF_4$ (26 mg, 0.23 mmol) were added to a solution of methanol (10 ml) and hexane (3 ml). The reaction mixture was degassed via three freeze/pump/thaw cycles, placed under an atmosphere of 100% ^{13}C labeled CO, and stirred for 72 h at room temperature. The solvent was removed under reduced pressure and the residue was rinsed well with hexane to yield the product, $[Ir(^{15}N\text{-}TPM)(H)(^{13}CO)(^{13}CO_2CH_3)]^+[BF_4]^-$ (**2**), as a pale grey powder (125 mg, 98% yield).

SPECTRAL DATA

Data for Compound **1,** *[Ru(TPM)(H)(CO)(PPh$_3$)]$^+$[BF$_4$]$^-$*

Chemical shifts (in ppm) (^1H, solvent d^6-acetone): 9.81 [$H_{1'}$], 8.68 [H_{5C}], 8.62 [H_{5A}], 8.57 [H_{5B}], 8.34 [H_{3A}], 7.70 [H_{Ph}^{para}], 7.61 [H_{Ph}^{ortho}], 7.55 [H_{Ph}^{meta}], 7.18 [H_{3C}], 6.86 [H_{3B}], 6.77 [H_{4A}], 6.63 [H_{4C}], 6.37 [H_{4B}], −12.10 [$H_{hydride}$]; (^{13}C, solvent d^6-acetone): 148.4 [C_{3A}], 148.3 [C_{3B}], 146.8 [C_{3C}], 135.2 [C_{5C}], 135.0 [C_{5B}], 134.7 [C_{Ph}^{meta}], 134.7 [C_{5A}], 131.7 [C_{Ph}^{para}], 129.6 [C_{Ph}^{ortho}], 109.4 [C_{4A}], 109.1 [C_{4C}], 108.8 [C_{4B}], 77.2 [$C_{1'}$]; (^{13}C, solvent d^8-THF): 206.4 [CO]; (^{31}P, solvent d^6-acetone): 64.9 [P_{Ph3}]; (^{15}N, solvent d^6-acetone, referenced to liquid ammonia (*13*)): 246.6 [N_{2C}], 242.4 [N_{2B}], 233.9 [N_{2A}], 208.3 [N_{1C}], 207.8 [N_{1A}], 207.1 [N_{1B}].

Coupling constants (in Hz) not shown in Fig. 1a (for visual clarity, one of the coupling partners is identified by underlining): J_{H3AH4A} |2.1|, J_{H3BH4B} |2.3|, J_{H3CH4C} |2.1|, J_{H4AH5A} |2.4|, J_{H4BH5B} |2.7|, J_{H4CH5C} |2.5|, J_{H3AN1A} −7.5, J_{H3BN1B} −7.6, J_{H3CN1C} −7.8, J_{H4AN1A} −6.1, J_{H4BN1B} −6.1, J_{H4CN1C} −6.2, J_{H5AN1A} −5.6, J_{H5BN1B} −5.8, J_{H5CN1C} −5.7, J_{HN1A} <|0.2|, J_{HN1B} 0.3, J_{HN1C} 0.7, J_{H3AN2A} 10.9, J_{H3BN2B} −10.4, J_{H3CN2C} −11.1, J_{H4AN2A} −2.1, J_{H4BN2B} −2.6, J_{H4CN2C} −2.2, J_{H5AN2A} −1.2, J_{H5BN2B} −1.4, J_{H5CN2C} −1.0, J_{N1AN2A} −10.0, J_{N1BN2B} −10.1, J_{N1CN2C} −10.8, J_{H3AP} 0.9, J_{H4AP} 0.8, J_{H5AP} 0.9, J_{PN1A} −1.4.

Data for Compound **2,** *[Ir(TPM)(H)(CO)(CO$_2$CH$_3$)]$^+$[BF$_4$]$^-$*

Chemical shifts (in ppm) (^1H, solvent d^8-THF): 9.89 [$H_{1'}$], 8.65 [H_{5C}], 8.65 [H_{5A}], 8.60 [H_{5B}], 8.42 [H_{3B}], 8.23 [H_{3C}], 8.18 [H_{3A}], 6.66 [H_{4C}], 6.64 [H_{4B}], 6.64 [H_{4A}], 3.60 [$H_{2'}$], −16.76 [$H_{hydride}$]; (^{13}C, solvent d^8-THF): 165.6 [C_1], 157.1 [C_2]; (^{13}C, solvent d^6-acetone): 148.8 [C_{3C}], 148.7 [C_{3B}], 147.1 [C_{3A}], 136.1 [C_{5B}], 135.9 [C_{5C}], 135.4 [C_{5A}], 110.1 [C_{4A}], 109.9 [C_{4C}], 109.5 [C_{4B}], 78.5 [$C_{1'}$], 51.9 [CH_3]; (^{15}N, solvent d^6-acetone, referenced to liquid ammonia (*13*)): 222.6 [N_{2C}], 208.8 [N_{2A}], 206.8 [N_{2B}], 205.5 [N_{1A}], 205.2 [N_{1C}], 204.5 [N_{1B}].

Coupling constants (in Hz) not shown in Fig. 1b (for visual clarity, one of the coupling partners is identified by underlining): J_{H3AN1A} −7.1, J_{H3BN1B} −6.9, J_{H3CN1C} −7.2, J_{H4AN1A} −6.1, J_{H4BN1B} −6.0, J_{H4CN1C} −5.9, J_{H5AN1A} −5.5, J_{H5BN1B} −5.7, J_{H5CN1C} −5.2, J_{H3AN2A} −10.2, J_{H3BN2B} −8.5, J_{H3CN2C} −9.9, J_{H4AN2A} −2.7, J_{H4BN2B} −3.2, J_{H4CN2C} −2.6, J_{H5AN2A} −1.6, J_{H5BN2B} −2.0, J_{H5CN2C} −1.5, J_{N1AN2A} −8.8, J_{N1BN2B} −7.8, J_{N1CN2C} −8.8, $|J_{C1N1B}|$ 0.5, $|J_{C2N1A}|$ 0.5.

RESULTS

Compounds and Spin Systems

The compounds investigated in the present study, [Ru(TPM)-(H)(CO)(PPh_3)]$^+$[BF_4]$^-$ and [Ir(TPM)(H)(CO)(CO_2CH_3)]$^+$[BF_4]$^-$, are shown in Fig. 1, together with an overview over the coupling constants measured across the metal centers. The tris(1-pyrazolyl)methane (TPM) ligand was uniformly enriched with ^{15}N. In addition, both carbonyl carbons in compound **2** were labeled with ^{13}C. None of the ruthenium or iridium isotopes carries a spin 1/2. Consequently, the presence of metal spins could be disregarded in the present study.

All coupling constants between nuclei in *trans* position with respect to the metal center are larger than 10 Hz and thus readily measured (Fig. 1). In contrast, *cis* couplings involving ^{15}N are at most 1.5 Hz. Quite generally, the coupling constants with ^{15}N tend to be relatively small. For example, $^2J_{HP}(cis)$ in compound **1** is larger than $^2J_{HN}(trans)$.

$^2J_{HN}$ and $^3J_{HN}$ coupling constants in the pyrazol rings of the free TPM ligand were measured earlier (*10*). They are larger than 5 Hz, both in the complexed and in the uncomplexed ligand. The $^1J_{NN}$ coupling in TPM varies between -7.5 and -13.0 Hz, depending on the state of ligation and the transition metal in the complex (*8, 10, 14, 15*). The negative sign of the $^1J_{NN}$ coupling was confirmed by a series of E.COSY-type experiments in free TPM as well as in a bis(1-pyralozyl) complex with Ru, by relating them to the sign of a one-bond ^{1}H–^{13}C coupling which can be assumed to be positive (*8, 10*). Since the magnitudes of the intrapyrazolyl J_{HN} and J_{NN} coupling constants are comparable in **1** and **2** to those previously observed in free TPM and in the Ru bis(1-pyrazolyl) complex (*8, 10*), it can be assumed that the $^1J_{NN}$ couplings in TPM are also negative in **1** and **2.** In the present work, the absolute signs of the coupling constants across the metal center were obtained by relating them to the sign of the $^1J_{NN}$ couplings.

Experiments Used for Analysis of Compound **1,** *[Ru(TPM)(H)(CO)(PPh_3)]$^+$[BF_4]$^-$*

The ^{15}N chemical shifts in **1,** [Ru(TPM)(H)(CO)(PPh_3)]$^+$[BF_4]$^-$, cluster into two groups, comprising N_{1A}–N_{1C} and N_{2A}–N_{2C}, respectively, with a larger chemical shift dispersion between N_{2A}, N_{2B} and N_{2C} (see Spectral Data). It was thus possible to selectively excite each group of spins separately. Furthermore, with a more selective pulse, a single one of the spins N_{2A}–N_{2C} could be excited. Similarly, the hydride resonance is well separated from the rest of the ^{1}H NMR spectrum, allowing the selective excitation of the hydride without disturbing any of the other proton resonances and vice versa. Selective pulses were used to reduce the spectral widths in the indirect frequency dimension and to refocus homonuclear couplings. Table 1 presents a survey over the experiments recorded and their information content.

^{15}N–HSQC–36N

^{15}N–HSQC–36N spectra yield ^{15}N–^{1}H cross peaks with an E.COSY-type appearence, correlating the sign of passive J_{NN} couplings in the F_1 frequency dimension with the sign of J_{HN} couplings in the F_2 dimension (*10*). In the same way, couplings with passive spins like ^{31}P lead to additional E.COSY-type multiplet splittings. The use of a ^{15}N inversion pulse selective for either the N_1 or N_2 spins, respectively, prevented the generation of unproductive three-spin terms like $H_xN_{1z}N_{2z}$, by restricting the evolution of the pyrazolyl protons during the INEPT period to a single intra-pyrazolyl J_{HN} coupling. In this way, all possible intra-pyrazolyl ^{1}H–^{15}N cross peaks were observed in two experiments, with the selective ^{15}N pulse set to invert either N_{1A}–N_{1C} or N_{2A}–N_{2C} (data not shown).

The three cross peaks observed between N_{2A}–N_{2C} and the hydride (denoted H) show that the sign of the *trans* coupling $J_{N2A\underline{P}}$ is opposite to that of the *cis* couplings $J_{N2B\underline{P}}$ and $J_{N2C\underline{P}}$ (Fig. 2a). Furthermore, the *cis* couplings $J_{N2B\underline{N2C}}$ an $J_{N2A\underline{N2C}}$ have the same sign as $J_{H\underline{N2C}}$, as measured from the N_{2B}–H and N_{2A}–H cross peaks. Since the sensitivity of the N_{2A}–H cross peak was low because of the small $J_{H\underline{N2A}}$ coupling, the measurement of $J_{N2A\underline{N2C}}$ was double checked later by DQ/ZQ and long-range ^{15}N–^{15}N (LRNN) experiments (see below).

$J_{H\underline{N1C}}$ (measured from the cross peak N_{2C}–H, Fig. 2a) was the only sizable coupling between the hydride and any of the N_1 spins which could be determined with confidence from the ^{15}N–HSQC–36N spectrum. Using an INEPT delay of 150 ms, the cross peak N_{1C}–H could be observed (Fig. 2b). The negative tilt of the cross peak shows that $J_{H\underline{N2C}}$ has the same sign as $J_{N1C\underline{N2C}}$; i.e., $\boldsymbol{J_{H\underline{N2C}}}$ **is negative** and, consequently, $\boldsymbol{J_{N2B\underline{N2C}}}$ **and** $\boldsymbol{J_{N2A\underline{N2C}}}$ **are negative.** Since N_{1A}–H and N_{1B}–H cross peaks could not be observed in ^{15}N–HSQC–36N experiments even after 12 h recording time, different experiments were required to obtain the sign information for the other two H–N_2 couplings across the metal center.

^{15}N–HSQC–36N with ^{15}N–^{15}N Relay

The cross peak N_{1B}–H was generated by transferring the magnetization from H to N_{2B} ($J_{H\underline{N2B}}$ = 1.3 Hz) and further to N_{1B} via a ^{15}N–^{15}N relay step ($J_{N2B\underline{N1B}}$ = -10.1 Hz), converting $N_{2By}H_z$ via the operators $N_{2Bx}N_{1Bz}H_z$ and $N_{2Bz}N_{1Bx}H_z$ into $N_{1By}H_z$ before the evolution time t_1. The cross peak (Fig. 2c) shows that $J_{H\underline{N2B}}$ has the opposite sign of $J_{N1B\underline{N2B}}$; i.e., $\boldsymbol{J_{H\underline{N2B}}}$ **is positive.** The cross peak N_{1A}–H could not be observed with this experiment, probably because $J_{H\underline{N1A}}$ is too small to allow the refocusing of $N_{1Az}H_y$ into observable magnetization.

^{31}P–HSQC

The cross peak P–H recorded in a conventional ^{31}P–HSQC spectrum relates the signs of $J_{P\underline{N2A}}$ and $J_{P\underline{N2C}}$ to those

TABLE 1

Experimental Schemes for the Determination of the Sizes and Relative Signs of Coupling Constants in Compound 1, [Ru(TPM)(H)(CO)(PPh$_3$)]$^+$[BF$_4$]$^-$

Experiment	Pulse Sequence[a]	Cross Peaks and Coherences[b]	Pairs of Coupling Constants Related[c]	Comments[d]
^{15}N-HSQC-36N [e]	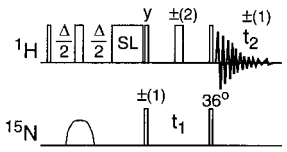	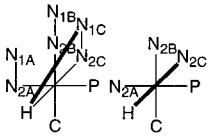	J_{N1CN2C} with J_{HN2C} J_{HP} with J_{N2CP}	Relates the sign of J_{HN} with $^1J_{NN}$ also for the pyrazolyl protons.
		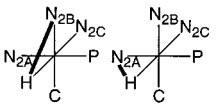	J_{HP} with J_{N2BP} J_{HP} with J_{N2AP}	
^{15}N-HSQC-36N with ^{15}N-^{15}N relay [f]	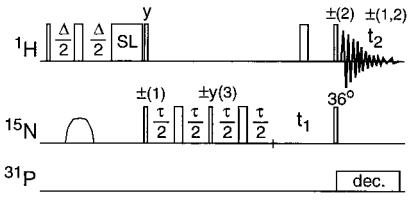	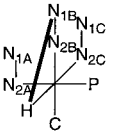	J_{N1BN2B} with J_{HN2B}	Generates the cross peak N_{1B}-H *via* the relay H → N_{2B} → N_{1B}.
^{31}P-HSQC [g]	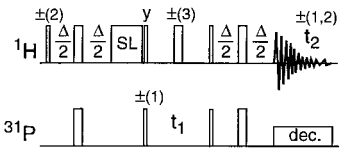	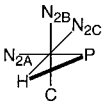	J_{PN2A} with J_{HN2A} J_{PN2C} with J_{HN2C}	Determines the sign of J_{HN2A}, since J_{PN2A} is related to J_{HP} and J_{HP} to J_{PN2C} (^{15}N-HSQC-36N), and J_{PN2C} is related to J_{HN2C} (^{31}P-HSQC).
LRNN [h]	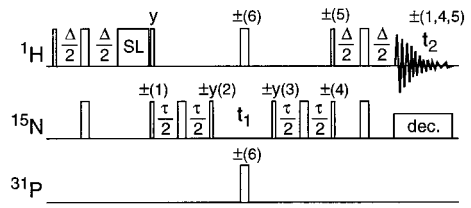	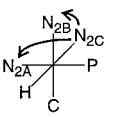		Generates the cross peaks N_{2A}-H and N_{2B}-H *via* the relay H → N_{2C} → N_{2A}, N_{2B}. Measures the size, not the sign, of the J_{NN} couplings. Identifies J_{NN} couplings across the methine group, too.
DQ/ZQ-HN(P) [i]	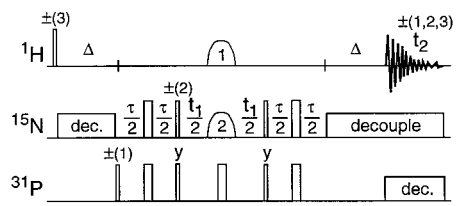	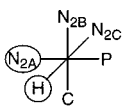	J_{N2AN2B} with J_{HN2B} J_{N2AN2C} with J_{HN2C}	Generates the coherence $H_yN_{2Ay}P_z$ *via* the relay H → P → N_{2A}.
DQ/ZQ-HN [j]	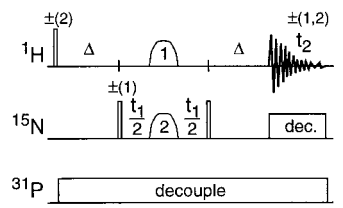	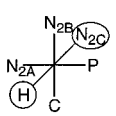	J_{N2CN2A} with J_{HN2A} J_{N2CN2B} with J_{HN2B}	Generates the coherence H_yN_{2Cy}.

TABLE 1—*Continued*

Experiment	Pulse Sequence[a]	Cross Peaks and Coherences[b]	Pairs of Coupling Constants Related[c]	Comments[d]
^{13}C-HMBC [k]	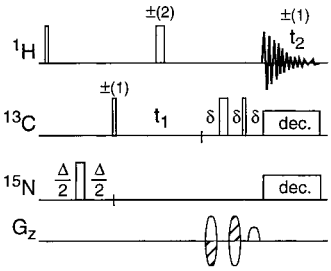	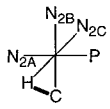	$J_{\underline{CN2C}}$ with $J_{\underline{HN2C}}$ $J_{\underline{CN2B}}$ with $J_{\underline{HN2B}}$ $J_{\underline{CP}}$ with $J_{\underline{HP}}$	
DQ/ZQ-CN [l]	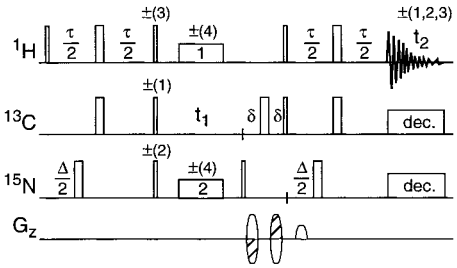	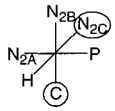	$J_{\underline{CP}}$ with $J_{\underline{N2CP}}$ $J_{\underline{CH}}$ with $J_{\underline{N2CH}}$	Generates the coherence $C_yN_{2Cy}H_z$ by simultaneous evolution of H under $J_{\underline{HC}}$ and $J_{\underline{HN2C}}$.

[a] Narrow and wide bars represent 90° and 180° pulses, respectively. SL denotes a spin-lock pulse of 1 ms duration. Boxes with lower amplitude of rectangular or rounded shape represent selective 180° pulses with a rectangular or more complicated shape, respectively. Broadband decoupling sequences are labeled "dec." Pulses are applied with phase x, unless indicated differently. Pulses which are phase alternated in the phase cycle are numbered and identified by ± signs. The same numbers are shown with the receiver phase, if the receiver phase is alternated together with the respective pulse phases. For example, the explicit phase cycle of the ^{15}N–HSQC–36N experiment with ^{15}N–^{15}N relay is 1st 90°(^{15}N) = 4(x, $-x$); 2nd 90°(^{15}N) = 4(y), 4($-y$); 90°(^{1}H) = 2(x, x, $-x$, $-x$); receiver = 2(x, $-x$, $-x$, x). E.COSY-type spectra were recorded with States–TPPI (*20*). DQ/ZQ experiments were recorded with the carrier frequency high field of the resonances participating in the mixed DQ/ZQ coherence.

[b] Bold lines connect the nuclei defining the chemical shifts of the cross peaks in the F_1 and F_2 dimensions of 2D correlation experiments. Cross peaks of the LRNN experiment are described by arrows pointing from the parent spin evolving during the delay τ to the spin to which antiphase magnetization is created by the J_{NN} coupling between the two ^{15}N spins. Circles identify the pairs of spins precessing as DQ and ZQ coherences during t_1 in DQ/ZQ experiments.

[c] For improved clarity, coupling constants are denoted with underlining one of the two nuclei involved in the coupling. Note that indices of the coupling constants can be swapped. For example, $J_{\underline{N2CP}}$ and $J_{\underline{PN2C}}$ denote the same coupling.

[d] Cartesian product operators (*28*) without signs or normalization factors are used to describe coherences.

[e] See Ref. (*8*). Shaped pulse: 4 ms hyperbolic secant (*29*) inversion pulse, acting on N_{2A}–N_{2C}. Δ = 150 ms, t_{1max} = 448 ms, t_{2max} = 1.25 s, total experimental time 3 h. In the experiment, where the selective pulse excited N_{1A}–N_{1C}: t_{1max} = 256 ms, total experimental time 1.5 h.

[f] Shaped pulse: 10 ms pulse with the shape of a Seduce element (*30*), acting on N_{2B}. Δ = 150 ms, τ = 50 ms, t_{1max} = 195 ms, t_{2max} = 1.18 s, total experimental time 8 h.

[g] See Refs. (*31, 32*). Δ = 18.6 ms, t_{1max} = 200 ms, t_{2max} = 1.19 s, total experimental time 0.5 h.

[h] See Refs. (*8, 17, 18, 33*). Δ = 50 ms, τ = 300 ms, t_{1max} = 97 ms, t_{2max} = 1.36 s, total experimental time 3.5 h.

[i] Shaped pulse 1: 1 ms hyperbolic secant inverting all protons but the hydride; shaped pulse 2: 4 ms hyperbolic secant inverting N_{1A}–N_{1C}. Δ = 18.6 ms, τ = 13.6 ms, t_{1max} = 1.28 s, t_{2max} = 1.15 s, total experimental time 2.3 h.

[j] Shaped pulses as in the DQ/ZQ–HN(P) experiment (footnote *i*). Δ = 27.7 ms, t_{1max} = 1.75 s, t_{2max} = 1.15 s, total experimental time 3.5 h.

[k] Δ = 58 ms, δ = 1.1 ms, t_{1max} = 480 ms, t_{2max} = 341 ms, total experimental time 6.4 h. Gradients: 2.5, −2.5, 5.0 G/cm (odd scans) or −2.5, 2.5, 5.0 G/cm (even scans), 1 ms duration each, sine-shaped.

[l] Selective pulse 1: 77 μs rectangular pulse inverting all protons but the hydride; selective pulse 2: 441 μs rectangular pulse inverting N_{1A}–N_{1C} but not N_{2C}. Δ = 27 ms, τ = 58 ms, δ = 1.1 ms, t_{1max} = 128 ms, t_{2max} = 983 ms, total experimental time 5.4 h. Gradients as in the ^{13}C–HMBC experiment (footnote *k*).

of $J_{\underline{HN2A}}$ and $J_{\underline{HN2C}}$, respectively (Fig. 2d). The couplings of P and H with N_{2B} are both small and therefore unresolved. The negative tilt of the cross peak shows that $\boldsymbol{J_{\underline{PN2C}}}$ **is positive,** since $J_{\underline{HN2C}}$ is negative. The N_{2C}–H cross peak in the ^{15}N–HSQC–36N spectrum showed that the sign of $J_{\underline{HP}}$ is opposite to that of $J_{\underline{PN2C}}$; i.e., $\boldsymbol{J_{\underline{HP}}}$ **is negative.** If $J_{\underline{HP}}$ is negative, $\boldsymbol{J_{\underline{PN2A}}}$ **is negative** and $\boldsymbol{J_{\underline{PN2B}}}$ **is positive** (from the N_{2A}–H and N_{2B}–H cross peaks in Fig. 2a, respectively). The correlation between $J_{\underline{PN2A}}$ and $J_{\underline{HN2A}}$ in the ^{31}P–HSQC spectrum shows that $\boldsymbol{J_{\underline{HN2A}}}$ **is positive.** Thus, all $^2J_{HN}(cis)$ and $^2J_{PN}(cis)$ couplings are positive, whereas $^2J_{HN}(trans)$ and $^2J_{PN}(trans)$ are negative.

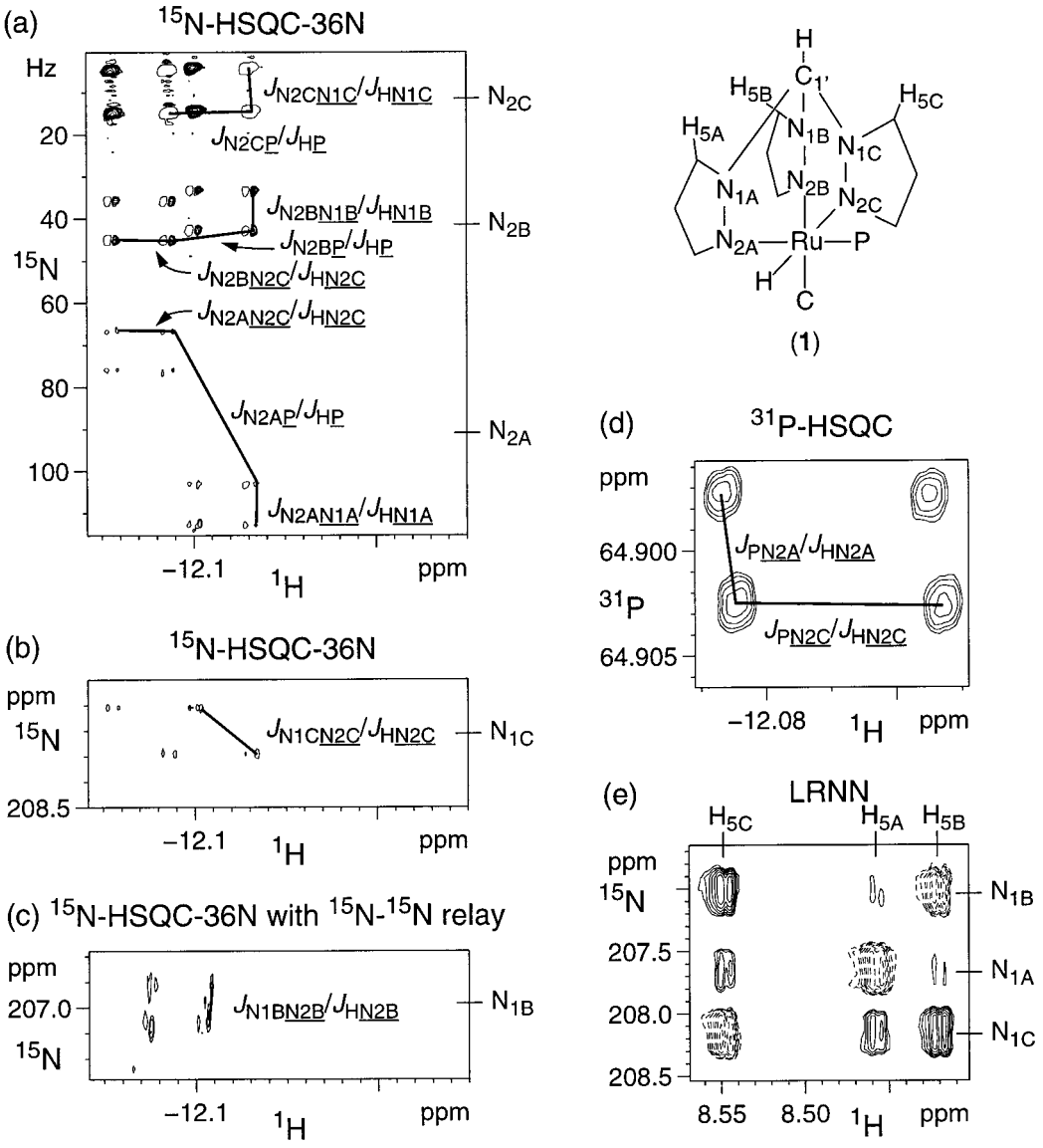

FIG. 2. Selected spectral regions from experiments recorded to determine the absolute sign of the ^2J coupling constants across the metal center in compound **1,** $[Ru(TPM)(CO)(H)(PPh_3)]^+[BF_4]^-$. The corresponding pulse sequences are shown in Table 1. Tilts of E.COSY-type cross peak multiplet fine structures are identified by lines which are labeled by the coupling constants responsible for the peak displacements; coupling constants measured from the peak displacements in the indirect frequency dimension are listed before the slash, those measured in the detection dimension after the slash. Positive and negative peaks are distinguished by plotting all contour levels or only the lowest one. In the quantitative long-range ^{15}N–^{15}N (LRNN) correlation spectrum (e), the distinction is made by solid and dashed lines. For reference, the chemical structure of **1** is shown with selected nuclei. The spectra were recorded at 25°C on a Bruker DMX 600 NMR spectrometer, using a 66 mM solution of **1** in d^8-THF for the ^{13}C–HMBC and DQ/ZQ–CN experiments, and a more dilute solution in d^4-methanol for all other spectra. (a) and (b) ^{15}N–HSQC–36N. The spectrum was folded in the F_1 frequency dimension. The two spectral regions shown were recorded using ^{15}N pulses selective for N_{2A-C} and N_{1A-C}, respectively (Table 1). (c) ^{15}N–HSQC–36N with ^{15}N–^{15}N relay. J_{HP} was decoupled for improved sensitivity. (d) ^{31}P–HSQC. (e) LRNN. $|J_{N1AN1B}| = 0.3$ Hz, $|J_{N1AN1C}| = 0.5$ Hz, and $|J_{N1BN1C}| = 0.8$ Hz were calculated from the relative peak intensities. Note that the spectrum yields two independent measurements for each J_{NN} coupling. (f) DQ/ZQ–HN(P). $F_{N2A} = 120$ Hz, $F_H = -51$ Hz. (g) DQ/ZQ–HN. $F_{N2C} = 109$ Hz, $F_H = -49$ Hz. (h) ^{13}C–HMBC. The multiplet fine structure is antiphase with respect to the J_{CP} and J_{HP} couplings, because the coupling evolution delay Δ used corresponded to an odd integer multiple of $1/(2J_{HP})$. (i) DQ/ZQ–CN. $F_C = -106$ Hz, $F_{N2C} = 37$ Hz.

LRNN

All $^2J_{NN}$ couplings across the metal center are 0.5 Hz or smaller. Their magnitude was measured using a quantitative long-range ^{15}N–^{15}N (LRNN) correlation experiment, where the size of the coupling constant is encoded in relative cross peak intensities (*10, 16–19*). The experiment is an "out-and-back" experiment with the magnetization transfer $H_y \rightarrow H_zN_{ay} \rightarrow H_zN_{az}N_{bx}$ and back (Table 1). The coupling con-

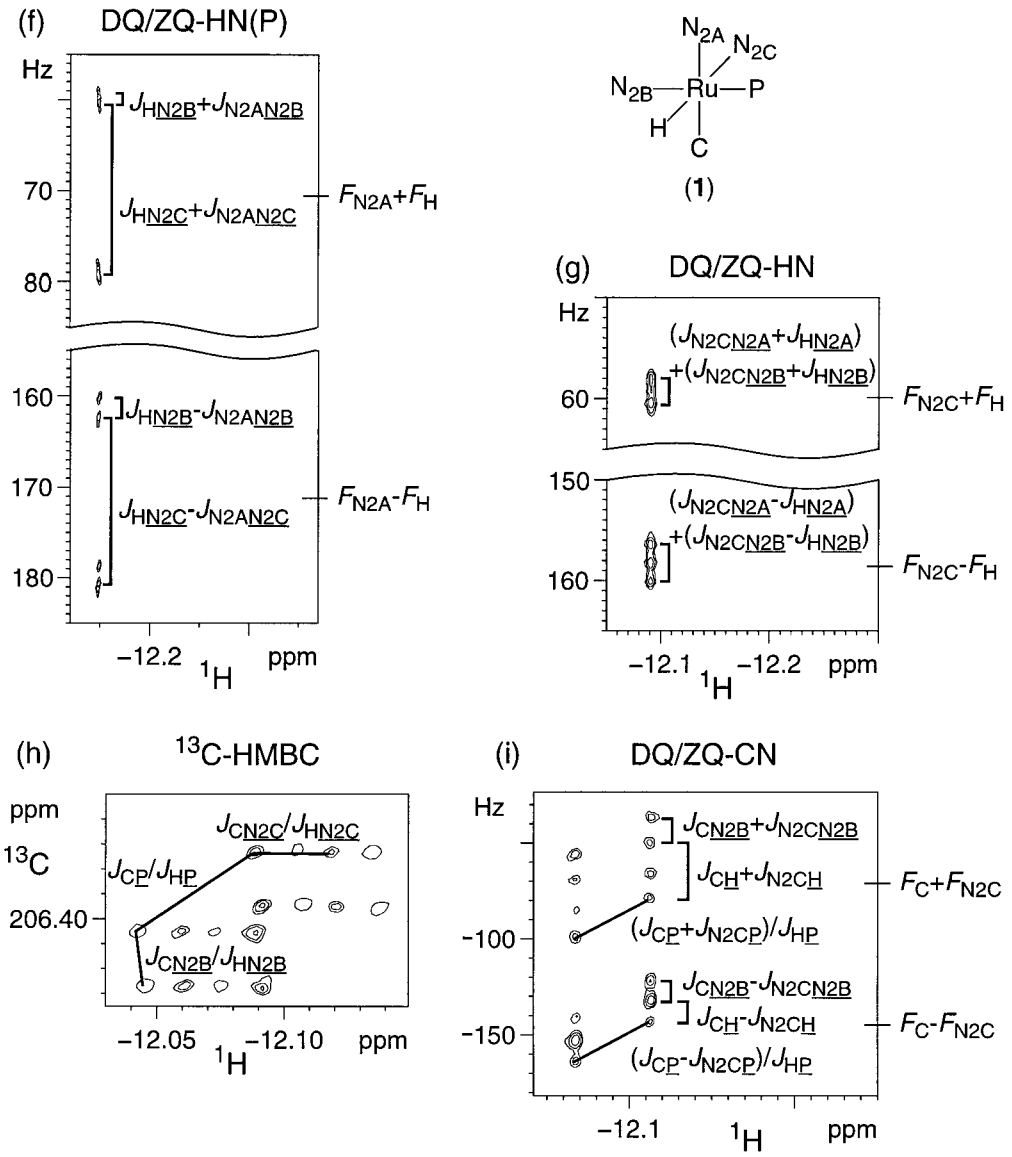

FIG. 2—*Continued*

stant J_{NN} is measured from the relative peak intensities of direct (N_a–H) and relayed (N_b–H) cross peaks: $I(N_b\text{–H})/I(N_a\text{–H}) = \sin^2(\pi J\tau)/\cos^2(\pi J\tau)$, where τ is the delay during which N_a partially evolves into antiphase magnetization with respect to N_b. To avoid reduced peak intensities from evolution under $^1J_{NN}$ couplings, τ was set to an integral multiple of $1/^1J_{NN}$. The experiment yielded $|J_{N2AN2B}| = 0.5$ Hz and $|J_{N2BN2C}| = 0.3$ Hz. Furthermore, the experiment demonstrated small couplings between the N_1 spins of different pyrazolyl rings which are presumably mediated by the $C_{1'}$ methine group (Fig. 2e).

DQ/ZQ–HN(P)

J_{N2AN2B} was determined from a DQ/ZQ experiment, where H and N_{2A} constituted the mixed DQ/ZQ coherence $H_yN_{2Ay}P_z$ which was generated via the intermediate terms H_xP_z, H_zP_x, and $H_zN_{2Az}P_y$. The relay via the phosphorus was favorable because the coupling constants J_{HP} and J_{PN2A} are relatively large (Fig. 1). The DQ (ZQ) coherence evolves with the sum (difference) of the couplings J_{HN2C} and J_{N2AN2C}. Since J_{HN2C} is large, the sign and size of the small J_{N2AN2C} coupling could be measured readily (Fig. 2f). In addition, the cross peaks were split by the sum (difference) of the couplings J_{HN2B} and J_{N2AN2B}. A selective 180°(^{15}N) pulse was applied to the group of N_1 resonances to prevent additional line splitting by $^1J_{N1AN2A}$. Similarly, the 180°(^{31}P) pulse in the middle of t_1 prevented the evolution under J_{N2AP} and J_{HP}. To refocus J_{HP} and J_{HN} couplings, the 180°(^{1}H) pulse in the middle of t_1 was applied as a semi-selective pulse, inverting all proton spins except for the hydride. Since the hydride

TABLE 2

Experimental Schemes for the Determination of the Sizes and Relative Signs of Coupling Constants in Compound 2, $[Ir(TPM)(H)(CO)(CO_2CH_3)]^+[BF_4]^-$

Experiment	Pulse Sequence[a]	Cross Peaks and Coherences[b]	Pairs of Coupling Constants Related[c]	Comments[d]
^{15}N-HSQC-36N [e]	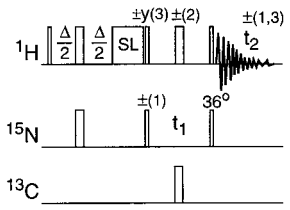	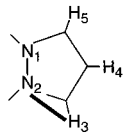	J_{H3N2} with J_{N1N2}	For all pyrazolyl rings.
DQ/ZQ-HH(N) [f]	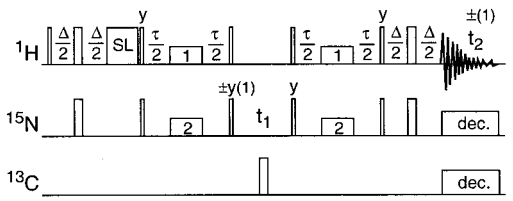	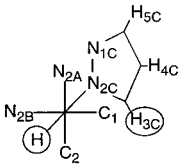	J_{HN2C} with J_{H3CN2C}	Generates the coherence $H_yH_{3Cy}N_{2Cz}$ *via* the relay $H \rightarrow N_{2C} \rightarrow H_{3C}$.
DQ/ZQ-HC(N) [g]	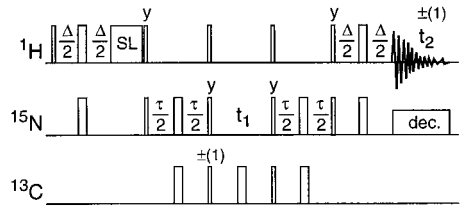	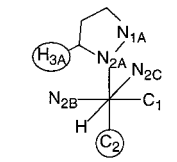	J_{C2N2A} with J_{H3AN2A} J_{C1N2B} with J_{H3BN2B}	Generates the coherences $H_{3Ay}C_{2y}N_{2Az}$ and $H_{3By}C_{1y}N_{2Bz}$ *via* the relays $H_{3A} \rightarrow N_{2A} \rightarrow C_2$ and $H_{3B} \rightarrow N_{2B} \rightarrow C_1$, respectively.
^{13}C-HSQC-36C [h]	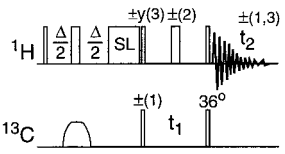	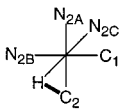 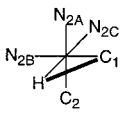	J_{C2C1} with J_{HC1} J_{C2N2C} with J_{HN2C} J_{C2N2A} with J_{HN2A} J_{C1C2} with J_{HC2} J_{C1N2C} with J_{HN2C} J_{C1N2B} with J_{HN2B}	
^{15}N-HSQC [i]	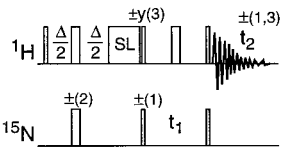	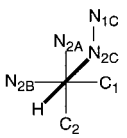	J_{N2CC1} with J_{HC1} J_{N2CC2} with J_{HC2} J_{N2CN1C} with J_{HN1C}	
DQ/ZQ-CN [j]	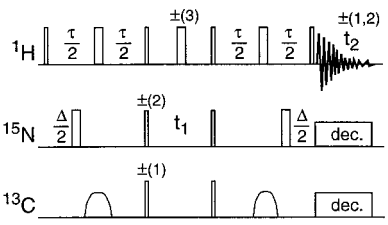	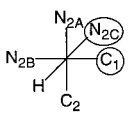 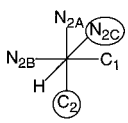	J_{N2CN2B} with J_{C1N2B} J_{N2CC2} with J_{C1C2} J_{N2CN2A} with J_{C2N2A} J_{N2CC1} with J_{C2C1}	Generates the coherence $N_{2Cy}C_{1y}H_z$ ($N_{2Cy}C_{2y}H_z$) by simultaneous evolution of H under J_{HN2C} and J_{HC1} (J_{HN2C} and J_{HC2}).

TABLE 2—*Continued*

Experiment	Pulse Sequence[a]	Cross Peaks and Coherences[b]	Pairs of Coupling Constants Related[c]	Comments[d]
DQ/ZQ-CN(C) [k]	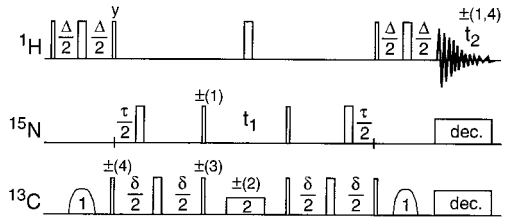	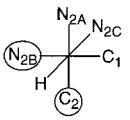	$J_{N2B\underline{N2A}}$ with $J_{C2\underline{N2A}}$	Generates the coherence $C_{2y}N_{2By}C_{1z}H_z$ *via* the relay $H \rightarrow C_1 \rightarrow C_2, N_{2B}$, using simultaneous evolution of C_1 under $J_{C1\underline{C2}}$ and $J_{C1\underline{N2B}}$.
LRCN [l]	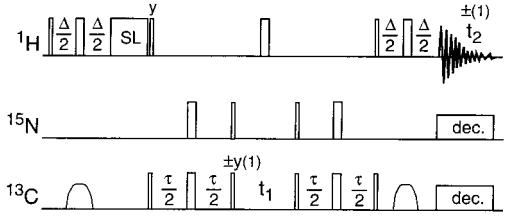	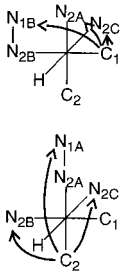		Generates the cross peaks N_2 - H *via* the relay $H \rightarrow C_1$ or $C_2 \rightarrow N_{2A}, N_{2B}, N_{2C}, N_{1B}, N_{1A}$, respectively. Measures the size, not the sign, of $J_{C1\underline{N2C}}, J_{C1\underline{N2A}}, J_{C1\underline{N1B}}$ and $J_{C2\underline{N2C}}, J_{C2\underline{N2B}}, J_{C2\underline{N1A}}$.
DQ/ZQ-CC [m]	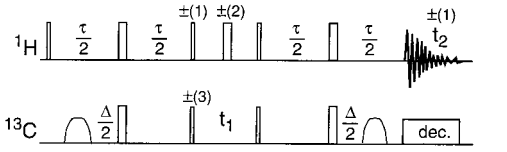	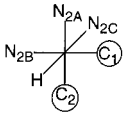	$J_{C1\underline{N2B}} + J_{C2\underline{N2A}}$ with $J_{C2\underline{N2B}} + J_{C1\underline{N2A}}$	Generates the coherence $C_{1y}C_{2y}H_z$ by simultaneous evolution of H under $J_{H\underline{C1}}$ and $J_{H\underline{C2}}$.

[a–d] For a definition of the symbols and conventions used, see the corresponding footnotes *a–d* of Table 1.

[e] See Ref. (*8*). Δ = 62.5 ms, t_{1max} = 256 ms, t_{2max} = 2.46 s, total experimental time 1.1 h.

[f] Δ = 17.9 ms, τ = 35.8 ms, t_{1max} = 164 ms, t_{2max} = 285 ms, experimental time 2.5 h, selective pulse 1: 4.81 ms rectangular 180° pulse for selective inversion of H_{3C} without exciting H_{5C}, selective pulse 2: 1.2 ms rectangular 180° pulse for selective refocusing of N_{2C} without exciting N_{1C}.

[g] Δ = 25 ms, τ = 122 ms, t_{1max} = 205 ms, t_{2max} = 570 ms, experimental time 0.5 h.

[h] See Ref. (*8*). Δ = 35.7 ms, t_{1max} = 512 ms, t_{2max} = 1.7 s, experimental time 1.2 h.

[i] See Refs. (*31, 32*). Δ = 62 ms, t_{1max} = 512 ms, t_{2max} = 2.9 s, experimental time 14 h.

[j] Δ = 9 ms, τ = 27.5 ms, t_{1max} = 2.05 s, t_{2max} = 570 ms, experimental time 11 h, selective pulse: 10 ms hyperbolic secant 180° inversion pulse. Correlations with C_1 and C_2 were obtained in separate experiments with the selective 180°(^{13}C) pulses applied to C_1 and C_2, respectively.

[k] Δ = 55.0 ms, τ = 27 ms, δ = 125 ms, t_{1max} = 2.05 s, t_{2max} = 570 ms, exp. time 5.7 h, selective pulse 1: 10 ms hyperbolic secant 180° pulse for selective inversion of C_1, selective pulse 2: 994 μs rectangular 180° pulse for selective inversion of C_1 without exciting C_2.

[l] See Ref. (*18*). Δ = 55 ms, τ = 262 ms, t_{1max} = 128 ms, t_{2max} = 524 ms, experimental time 0.5 h, selective pulse: 10 ms hyperbolic secant 180° inversion pulse. Correlations with C_1 and C_2 were obtained in separate experiments with the selective 180°(^{13}C) pulses applied to C_1 and C_2, respectively. The correlations with C_2 were measured in 2 h on a more dilute sample. The phases of all ^{13}C and ^{15}N pulses preceding t_1 were simultaneously incremented by the States–TPPI scheme (*20*).

[m] Δ = 55 ms, τ = 125 ms, t_{1max} = 1 s, t_{2max} = 570 ms, experimental time 9 h, selective pulse: 10 ms hyperbolic secant 180° pulse for selective inversion of C_1.

resonance appears as a singlet in the presence of ^{15}N and ^{31}P decoupling, refocusing of the transverse proton magnetization was not necessary to obtain a purely absorptive ^{1}H signal. The spectrum (Fig. 2f) shows that the sum of $J_{H\underline{N2B}}$ and $J_{N2A\underline{N2B}}$ is smaller than the difference, showing that $\boldsymbol{J_{N2A\underline{N2B}}}$, unlike $J_{H\underline{N2B}}$, **is negative**. In contrast, the sum of $J_{H\underline{N2C}}$ *and* $J_{N2A\underline{N2C}}$ is larger than the difference, showing that $\boldsymbol{J_{N2A\underline{N2C}}}$, like $J_{H\underline{N2C}}$, **is negative**.

DQ/ZQ–HN

The sign of $J_{N2B\underline{N2C}}$ was determined from a DQ/ZQ–HN experiment, where mixed DQ/ZQ coherence was prepared between H and N_{2C}. Couplings to N_1 spins were refocused by a selective 180°(^{15}N) pulse inverting the N_1 spins, and couplings to protons other than the hydride were refocused by a selective 180°(^{1}H) pulse applied to all protons except

the hydride resonance. Together with ^{31}P broadband decoupling, the couplings to N_{2A} and N_{2B} were the only unrefocused couplings. Therefore, the DQ peak is split both by $J_{N2CN2B} + J_{HN2B}$ and $J_{N2CN2A} + J_{HN2A}$, and the ZQ peak by $J_{N2CN2B} - J_{HN2B}$ and $J_{N2CN2A} - J_{HN2A}$. The signs and magnitudes of all these couplings are known, except for the sign of J_{N2CN2B}. Although the couplings are incompletely resolved in the experimental cross peaks (Fig. 2g), the separation between the outermost multiplet components is clearly bigger for the ZQ than for the DQ cross peak. Thus, $|J_{N2CN2A} - J_{HN2A} + J_{N2CN2B} - J_{HN2B}| > |J_{N2CN2A} + J_{HN2A} + J_{N2CN2B} + J_{HN2B}|$ or $|J_{N2CN2B} - 3.0\ \text{Hz}| > |J_{N2CN2B} + 2.6\ \text{Hz}|$. According to the LRNN experiment, the magnitude of J_{N2CN2B} is 0.3 Hz. Thus, $\boldsymbol{J_{N2CN2B}}$ **is negative,** like all the other $^2J_{NN}$ couplings across the metal center of compound **1.**

^{13}C–HMBC

Coupling constants with the carbonyl carbon were measured at natural isotopic abundance. A ^{13}C–HMBC spectrum (Fig. 2h), recorded with pulsed field gradients for coherence selection, shows that $\boldsymbol{J_{CN2B}}$ **is negative** (negative tilt and positive J_{HN2B}), $\boldsymbol{J_{CP}}$ **is negative** (positive tilt and negative J_{HP}), and $\boldsymbol{J_{CN2C}}$ **is positive** (negative tilt and negative J_{HN2C}). The magnitude of the active coupling J_{HC} is 9.6 Hz, but its sign cannot be determined from this experiment.

DQ/ZQ–CN

This experiment determined the sign of J_{HC} by relating it to the sign of J_{HN2C} (Fig. 2i). The mixed DQ/ZQ coherence involved the ^{13}C spin of the carbonyl and the ^{15}N spin of N_{2C}. Couplings to N_1 spins were refocused by a selective 180°(^{15}N) pulse inverting the N_1 spins and couplings to protons other than the hydride were refocused by a selective 180°(^{1}H) pulse applied to all protons except the hydride resonance. The remaining couplings in the indirect frequency dimension include couplings to H, P, N_{2A}, and N_{2B}. J_{CN2A} and J_{N2CN2A} are both small and not resolved in the multiplet fine structure (Fig. 2i). The couplings to ^{31}P are resolved in an E.COSY-type displacement of the multiplet fine structure of the DQ and ZQ cross peaks. The remaining couplings to H and N_{2B} give rise to a doublet of doublets. The largest splitting, representing $J_{CH} + J_{N2CH}$, is observed for the DQ cross peak. Since J_{N2CH} is negative, $\boldsymbol{J_{CH}}$ **is negative.**

Completeness of J-Coupling Measurements in Compound **1,** *[Ru(TPM)(H)(CO)(PPh$_3$)]$^+$[BF$_4$]$^-$*

J_{CN2A} was the only two-bond coupling across the metal center which was not determined by the present set of experiments. From the ^{13}C linewidth in the ^{13}C–HMBC spectrum of Figure 2h, $|J_{CN2A}|$ was estimated to be smaller than 1.5 Hz. In principle, J_{CN2A} could be measured by a DQ/ZQ–PC experiment, where ^{13}C and ^{31}P constitute the DQ/ZQ coherence evolving during the evolution time. This experiment would correlate the small J_{CN2A} coupling with the large J_{PN2A} coupling. Starting from the hydride, the coherence $P_yC_yH_z$ can easily be generated by simultaneous evolution of H under the relatively large couplings J_{HP} and J_{HC}. In practice, the experiment failed because of signal-to-noise limitations imposed by the low natural abundance of ^{13}C and the rapid transverse relaxation rate of the ^{31}P spin. The problems from ^{31}P relaxation could be alleviated by the use of the DQ/ZQ–HN(P) experiment (Table 1), where ^{31}P evolves only during relatively short relay periods. In this experiment, J_{N2AC} would be correlated with J_{HC}, but the sensitivity was insufficient to perform this experiment at natural ^{13}C abundance.

Experiments Used for Compound **2,** *[Ir(TPM)(H)(CO)(CO$_2$CH$_3$)]$^+$[BF$_4$]$^-$*

In contrast to compound **1,** [Ru(TPM)(H)(CO)(PPh$_3$)]$^+$[BF$_4$]$^-$, the ^{15}N chemical shifts of N_{1A}–N_{1C} and N_{2A}–N_{2C} in compound **2,** [Ir(TPM)(H)(CO)(CO$_2$CH$_3$)]$^+$[BF$_4$]$^-$, did not cluster into two groups which could have been selectively excited in a simple way (see Spectral Data). Furthermore, the $^2J_{HN}(cis)$ couplings were smaller in **2** than in **1,** so that only a single ^{15}N–^{1}H correlation peak could be generated with the hydride resonance (which is well resolved at −16.76 ppm) in ^{15}N–HSQC experiments. On the other hand, both carbonyl groups were labeled with ^{13}C, extending the range of possible experiments. Thus, the sign and size of all 15 ^2J coupling constants across the metal center could be determined. Table 2 presents a survey over the experiments recorded and their information content.

^{15}N–HSQC–36N

The signs of the large couplings J_{HN2C}, J_{C1N2B}, and J_{C2N2A} across the metal center were determined by relating them to those of the intra-pyrazolyl $^2J_{H3N2}$ couplings. The signs of the $^2J_{H3N2}$ couplings were in turn related to the signs of the $^1J_{N1N2}$ couplings by a ^{15}N–HSQC–36N spectrum recorded with decoupling of J_{CN} couplings. The negative tilt of the cross peaks in Fig. 3a shows that the $\boldsymbol{^2J_{H3N2}}$ **(and** $\boldsymbol{^3J_{H3N1}}$**) couplings are negative** for all pyrazolyl rings, because they are of the same sign as $^1J_{N1N2}$.

DQ/ZQ–HH(N)

The sign of J_{HN2C} was determined from a DQ/ZQ–HH(N) experiment, where the hydride and H_{3C} proton were involved in the mixed DQ/ZQ coherence $H_yH_{3Cy}N_{2Cz}$. This coherence was prepared starting from magnetization of the hydride, via the intermediate terms H_y, H_xN_{2Cz}, H_zN_{2Cy}, and $H_zH_{3Cz}N_{2Cx}$. During the relay period τ, couplings between N_{2C} and H_{5C} were refocused by a selective 180°(^{1}H) inversion pulse acting on H_{3C} but not on H_{5C} or the hydride. J_{N2CN1C} was refocused by a selective 180°(^{15}N) refocusing pulse acting on N_{2C} but not on

N_{1C}. J_{HN2C} is the largest J_{HN} coupling with the hydride resonance and all intra-pyrazolyl J_{HH} couplings are small. Figure 3b shows that J_{HN2C} has the same sign as J_{H3CN2C}; i.e., $\boldsymbol{J_{HN2C}}$ **is negative.**

DQ/ZQ–HC(N)

The sign of the other two *trans* metal couplings, J_{N2AC2} and J_{N2BC1}, was determined by a DQ/ZQ experiment, where the carbonyl carbons C_1 and C_2 formed a DQ/ZQ coherence with the H_3 proton from the pyrazolyl group on the opposite side of the metal center. The coherence $H_{3Ay}C_{2y}N_{2Az}$ was prepared starting from H_{3A} magnetization, H_{3Ay}, via the intermediate terms $H_{3Ax}N_{2Az}$, $H_{3Az}N_{2Ay}$, and $H_{3Az}C_{2z}N_{2Ax}$. The corresponding pathway starting from H_{3B} yielded DQ/ZQ coherence between H_{3B} and C_1. The relay period τ was set to $1/^1J_{NN}$ to avoid defocusing of the N_2 magnetizations with respect to the N_1 spins. Figure 3c shows that J_{C2N2A} (J_{C1N2B}) and J_{H3AN2A} (J_{H3BN2B}) have the same sign. Thus, $\boldsymbol{J_{C2N2A}}$ **and** $\boldsymbol{J_{C1N2B}}$ **are negative.**

^{13}C–HSQC–36C

Both C_1 and C_2 yielded cross peaks with the hydride resonance in a ^{13}C–HSQC spectrum. In the absence of ^{15}N decoupling, E.COSY-type cross peaks were obtained with respect to couplings with ^{15}N. With a 36°(^{13}C) pulse at the end of the evolution time t_1, J_{CC} and J_{HC} couplings result in E.COSY-type multiplet splittings, too (*8, 10*). The spectrum shows that J_{C2N2C} and J_{C1N2C} have the opposite sign from J_{HN2C}; i.e., $\boldsymbol{J_{C2N2C}}$ **and** $\boldsymbol{J_{C1N2C}}$ **are positive** (Fig. 3d). Furthermore, $\boldsymbol{J_{HN2A}}$ **and** $\boldsymbol{J_{HN2B}}$ **are positive,** as their correlation with the negative J_{C2N2A} and J_{C1N2B} couplings resulted in a negative tilt in the multiplet fine structures of the respective cross peaks.

^{15}N–HSQC

A simple ^{15}N–HSQC spectrum yields a single cross peak with the hydride resonance, with J_{HN2C} as the active coupling. In the absence of ^{13}C decoupling and with a 90°(^{15}N) pulse after the evolution time t_1, an E.COSY-type multiplet fine structure is observed with respect to the ^{13}C spins (Fig. 3e). The tilts in the cross peak show that the signs of J_{HC1} and J_{HC2} are opposite to those of J_{N2CC1} and J_{N2CC2}, respectively; i.e., $\boldsymbol{J_{HC1}}$ **and** $\boldsymbol{J_{HC2}}$ **are negative.**

DQ/ZQ–CN

The ^{13}C–HSQC–36C spectrum showed that J_{HC1} and J_{HC2} have the same sign as J_{C1C2} (Fig. 3d). The absolute sign of J_{C1C2} is determined by a DQ/ZQ–CN experiment, where C_1 and N_{2C} constitute the mixed DQ/ZQ coherence. The experiment differs from the DQ/ZQ–CN experiment used for compound **1** (Table 2) mainly by the absence of gradient pulses and the use of selective 180°(^{13}C) pulses to restrict the evolution to J_{HC1} during the INEPT periods. Starting from magnetization of the hydride, H_y, the term $H_yN_{2Cz}C_{1z}$ is generated and converted into the mixed DQ/ZQ coherence $N_{2Cy}C_{1y}H_z$. This coherence evolves during t_1 under J_{NN}, J_{CC}, and J_{CN} couplings. The cross peaks observed at $F_{N2C} \pm F_{C1}$ show that J_{C1C2} is opposite in sign to J_{N2CC2}; i.e., $\boldsymbol{J_{C1C2}}$ **is negative** (Fig. 3f). Furthermore, the cross peaks show that J_{N2CN2B} has the same sign as J_{C1N2B}. Since J_{C1N2B} is negative, $\boldsymbol{J_{N2CN2B}}$ **is negative.**

In a completely analogous way, a DQ/ZQ–CN experiment with C_2 instead of C_1 in the mixed DQ/ZQ coherence shows that $\boldsymbol{J_{N2CN2A}}$ **is negative,** too (Fig. 3g). At this point, all *cis* couplings except J_{N2AN2B}, J_{C1N2A}, and J_{C2N2B} have been measured and their signs determined.

DQ/ZQ–CN(C)

The sign of J_{N2AN2B} was determined by a DQ/ZQ experiment, where C_2 and N_{2B} precessed in the mixed DQ/ZQ coherence $C_{2y}N_{2By}C_{1z}H_z$. This coherence was generated starting from magnetization of the hydride, H_y, with the intermediate terms H_xC_{1z}, H_zC_{1y}, $H_zC_{1y}C_{2z}N_{2Bz}$ (Table 2). For optimum magnetization transfer, a selective 180°(^{13}C) inversion pulse was applied to C_1 during the delay Δ. J_{NN} and J_{CN} were active couplings during the evolution time t_1. J_{C1C2} was refocused by a selective 180°(^{13}C) inversion pulse applied to C_1 in the middle of t_1. The spectrum shows that J_{N2BN2A} has the same sign as J_{C2N2A} (Fig. 3h). Since J_{C2N2A} is negative, $\boldsymbol{J_{N2BN2A}}$ **is negative.**

LRCN

The size of J_{C1N2A} and J_{C2N2B} was readily determined by quantitative long-range ^{13}C–^{15}N (LRCN) correlation experiments, which encode the magnitude of the coupling constants in relative cross peak intensities (*10, 16–19*). The experiment

FIG. 3. Selected spectral regions from experiments recorded to determine the absolute sign of the ^2J coupling constants across the metal center in compound **2,** [Ir(TPM)(H)(CO)(CO_2CH_3)]$^+$[BF_4]$^-$. The same labeling conventions as those in Fig. 2 were used. The frequency axis of DQ/ZQ cross peaks, which are shown in cross sections along the indirect frequency dimension, (f), (g), (h), and (k), displays only the double-quantum frequencies (the zero-quantum frequencies are higher in the DQ/ZQ–CN and DQ/ZQ–CN(C) experiments and lower in the DQ/ZQ–CC experiment). All but one of the spectra were recorded on a Bruker DRX 400 NMR spectrometer, using a 15 mM sample of **2** in THF-d^8 at 27°C. (a) ^{15}N–HSQC–36N. The N_{2C} signal is folded ($\delta(N_{2C})$ = 222.6 ppm). (b) DQ/ZQ–HH(N). F_{H3C} = −10247 Hz, F_H = −257 Hz. (c) DQ/ZQ–HC(N). F_{H3A} = −88 Hz, F_{C2} = −38 Hz; F_{H3B} = −880 Hz, F_{C1} = −190 Hz. The doublet fine structure of the zero-quantum peaks is not resolved. (d) ^{13}C–HSQC–36C. The spectrum was folded in the F_1 frequency dimension. (e) ^{15}N–HSQC. (f) DQ/ZQ–CN. F_{N2C} = 69 Hz, F_{C1} = −32 Hz. (g) DQ/ZQ–CN. F_{N2C} = 69 Hz, F_{C2} = −46 Hz. (h) DQ/ZQ–CN(C). F_{N2B} = 77 Hz, F_{C2} = −35 Hz. (i) Quantitative long-range ^{13}C–^{15}N (LRCN) correlation experiment with C_1. The labeling of the F_1 frequency axis pertains only to the ^{15}N chemical shifts. (j) LRCN correlation experiment showing the correlations with C_2. The spectrum was recorded at 600 MHz ^{1}H frequency. (k) DQ/ZQ–CC. F_{C1} = −880 Hz, F_{C2} = −35 Hz.

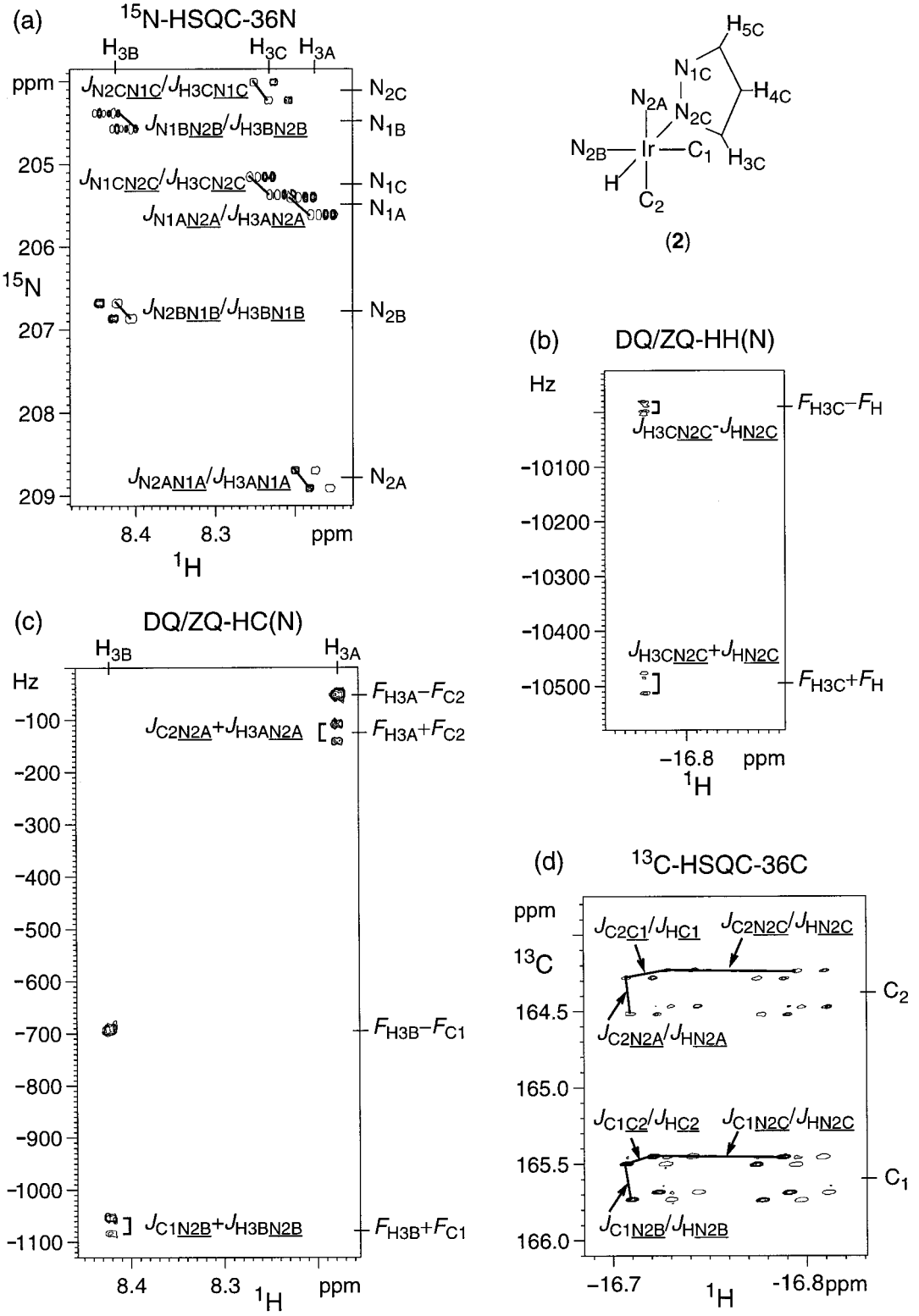
(a)
15N-HSQC-36N
H3B
H3C
H3A
ppm
JN2CN1C/JH3CN1C
JN1BN2B/JH3BN2B
JN1CN2C/JH3CN2C
JN1AN2A/JH3AN2A
JN2BN1B/JH3BN1B
JN2AN1A/JH3AN1A
N2C
N1B
N1C
N1A
N2B
N2A
205
206
15N
207
208
209
8.4
8.3
ppm
1H
H5C
N1C
H4C
N2A
N2C
N2B
Ir
C1
H3C
H
C2
(2)
(b)
DQ/ZQ-HH(N)
Hz
JH3CN2C-JHN2C
FH3C−FH
-10100
-10200
-10300
-10400
-10500
JH3CN2C+JHN2C
FH3C+FH
−16.8
ppm
1H
(c)
DQ/ZQ-HC(N)
H3B
H3A
Hz
FH3A−FC2
JC2N2A+JH3AN2A
FH3A+FC2
-100
-200
-300
-400
-500
-600
-700
-800
-900
-1000
-1100
FH3B−FC1
JC1N2B+JH3BN2B
FH3B+FC1
8.4
8.3
1H
ppm
(d)
13C-HSQC-36C
ppm
13C
JC2C1/JHC1
JC2N2C/JHN2C
JC2N2A/JHN2A
C2
164.5
165.0
JC1C2/JHC2
JC1N2C/JHN2C
JC1N2B/JHN2B
165.5
C1
166.0
−16.7
1H
-16.8ppm

FIGURE 3

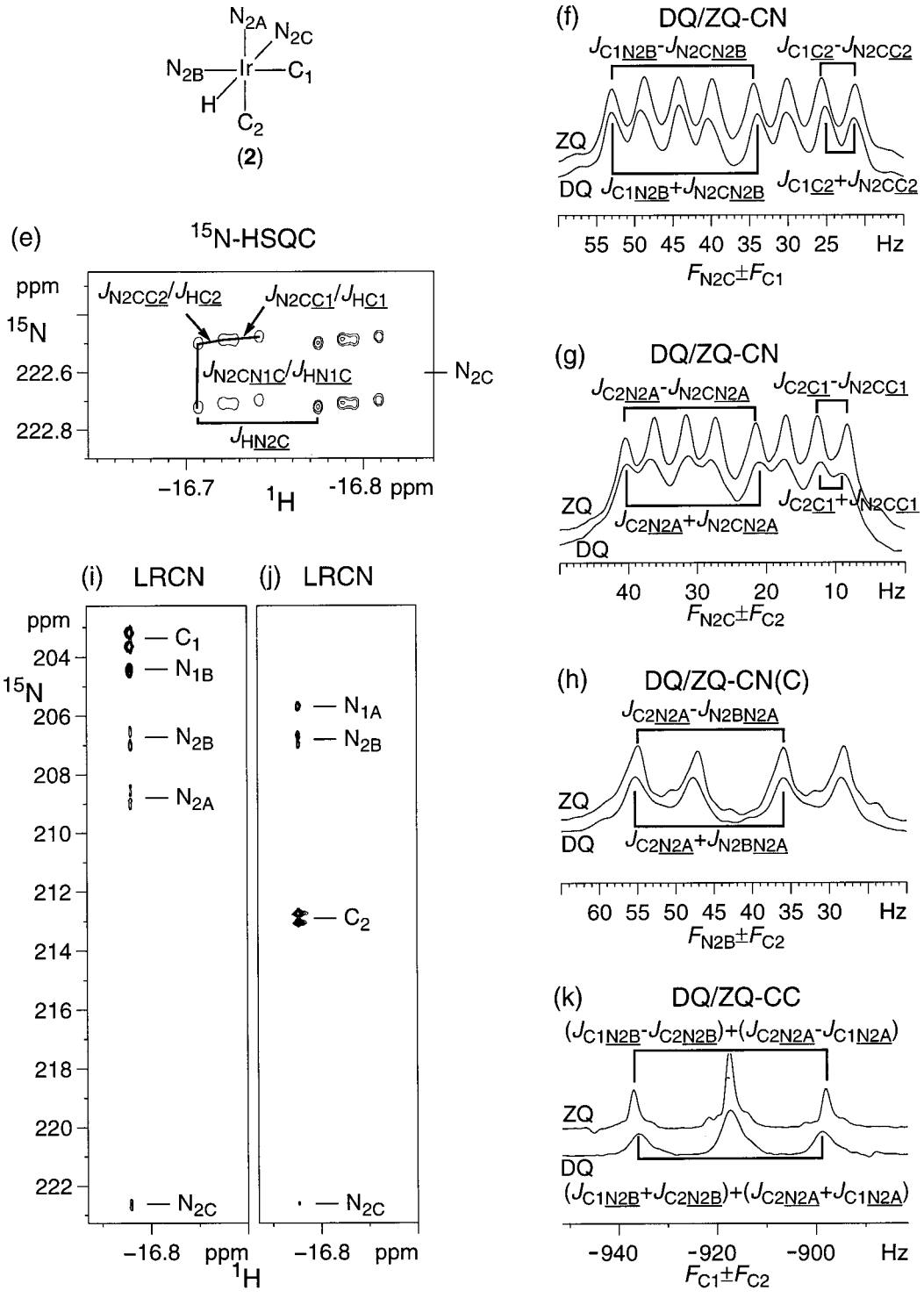

FIG. 3—*Continued*

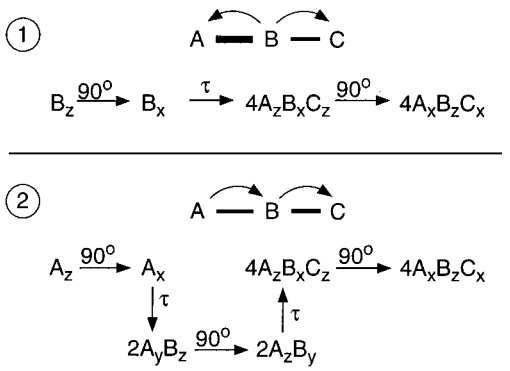

FIG. 4. Two alternative magnetization transfer pathways for the generation of DQ/ZQ coherence suitable for the determination of the relative signs of J_{AB} and J_{BC} in a linear spin system A–B–C. The pathways are indicated with Cartesian product operators (*28*). 90° pulses are assumed to be non-selective. τ denotes a coupling evolution delay. The term $4A_xB_zC_x$ represents the desired mixed DQ/ZQ coherence between the spins A and C, precessing under scalar couplings to the common coupling partner B. Measurement of J_{AB} and J_{BC} from the DQ/ZQ cross peaks is simplified, if one of the coupling constants is large (*22*). In many of the DQ/ZQ experiments of Tables 1 and 2, DQ/ZQ coherences between spins A and C are generated via relatively large couplings with spins outside the A–B–C spin system, allowing the sensitive measurement of very small J_{AB} or J_{BC} couplings.

used for measuring the small J_{CN} couplings with C_1 was performed using the magnetization transfer $H_y \rightarrow H_xC_{1z} \rightarrow H_zC_{1y} \rightarrow H_zC_{1x}N_z \rightarrow H_zC_{1z}N_y$ and back. Magnetization which has not evolved during the delay τ with respect to J_{CN} couplings continues to precess during t_1 as H_zC_{1y}. The coupling constant J_{C1N2A} was measured from the relative peak intensities of the direct (C_1–H) and the relayed (N_{2A}–H) cross peaks: $I(C_1\text{–H})/I(N_{2A}\text{–H}) = \sin^2(\pi J\tau)/\cos^2(\pi J\tau)$. To avoid reduced peak intensities from evolution under J_{C1C2} and J_{C1N2B}, τ was set close to $1/J_{C1C2} \approx 3/J_{C1N2B}$. The experiment yielded $|J_{C1N2A}| =$ 0.4 Hz and $|J_{C1N1B}| = 0.5$ Hz, and confirmed the size of J_{C1N2C} (Fig. 3i). The corresponding LRCN experiment for measuring J_{CN} couplings with C_2 was obtained by applying the selective 180°(^{13}C) inversion pulse to C_2 instead of C_1 (Fig. 3j). The experiment yielded $|J_{C2N2B}| = 0.5$ Hz and $|J_{C2N1A}| = 0.5$ Hz.

DQ/ZQ–CC

The sign of the couplings J_{C1N2A} and J_{C2N2B} was determined from a DQ/ZQ–CC experiment, with C_1 and C_2 constituting the mixed DQ/ZQ coherence. The coherence $C_{1y}C_{2y}H_z$ was generated by evolution of the magnetization of the hydride, H_y, under the couplings J_{HC1} and J_{HC2}, yielding $H_yC_{1z}C_{2z}$ at the end of the delay τ. Since J_{HC1} is significantly larger than J_{HC2}, a selective 180°(^{13}C) inversion pulse was applied to C_1 during the delay τ to shorten the effective defocusing period for J_{HC1}. With $\tau = 1/(2J_{HC2})$ and $\Delta = 1/(2J_{HC1})$, H_y evolves into $H_yC_{1z}C_{2z}$ with optimum efficiency. The DQ/ZQ coherence evolves during t_1 with respect to J_{CN} couplings. Since J_{C1N2B} and J_{C2N2A} are very similar and all other J_{CN} couplings are small, the resulting multiplet fine structures of the DQ and ZQ cross peaks appear as triplets (Fig. 3k). The separation of the outer components is $(J_{C1N2B} + J_{C2N2B}) + (J_{C2N2A} + J_{C1N2A}) = -37.1$ Hz for the DQ cross peak and $(J_{C1N2B} - J_{C2N2B}) + (J_{C2N2A} - J_{C1N2A}) = -38.9$ Hz for the ZQ cross peak. The difference in the total multiplet splitting is $2(J_{C2N2B} + J_{C1N2A}) = 1.8$ Hz. Since the sizes of these two couplings are 0.5 and 0.4 Hz, respectively, according to the LRCN spectra, **J_{C1N2A} and J_{C2N2B} are both positive.**

DISCUSSION

The two-bond coupling constants measured across the metal center of both compounds investigated here obey the sign rule $^2K(trans) > 0$ and $^2K(cis) < 0$ (Fig. 1). The sign rule holds likewise for the Ru complex investigated earlier (*10*). The rule could be verified for couplings between ^{1}H, ^{15}N, ^{13}C, and ^{31}P spins in different configurations and was found to hold even for very small $J_{NN}(cis)$ and $J_{CN}(cis)$ couplings. The absolute sign of the coupling constants across a metal center is thus a useful parameter for the identification of ligand conformations in transition metal complexes.

The E.COSY-type and DQ/ZQ experiments presented here facilitate the measurement of the absolute signs of coupling constants. Traditionally, such measurements have been performed by INDOR-type double resonance experiments (*6*), which can be difficult to perform for small coupling constants. Although the present study exclusively used 2D NMR data for coupling constant measurements, the total experimental time for each compound amounted to less than 2 days.

E.COSY-type spectra usually contain more than a single cross peak, allowing the measurement of several coupling constants from the same data set. In the present study, most of the E.COSY-type spectra were folded in the indirect frequency dimension to combine high resolution with short recording times. The States–TPPI scheme was used for quadrature detection (*20*) to make sure that the apparent tilt of the E.COSY-type cross peaks was not affected by folding. The main drawback of E.COSY spectra is that they cannot provide sign information for coupling constants in linear spin systems.

The problem of determining the relative signs of coupling constants in a linear spin system is resolved by DQ/ZQ experiments (*21*). Although DQ/ZQ experiments tend to require tailored 2D NMR experiments for each pair of selected coupling constants which are to be related to each other, a set of tailored experiments may be faster to record than a single non-selective experiment, since the desired line splitting can usually be observed in cross peaks with fewer peaks in the multiplet fine structure. The advantage of DQ/ZQ experiments over E.COSY-type experiments with small active couplings is demonstrated by the determination of the signs of the large $^2J(trans)$ couplings across the metal center in compounds **1** and **2**: trying to generate ^{15}N–HSQC cross peaks via the small three-bond coupling constants between the hydride and the N_1 spins of TPM in **1** (Table 1, Fig. 2) was much more

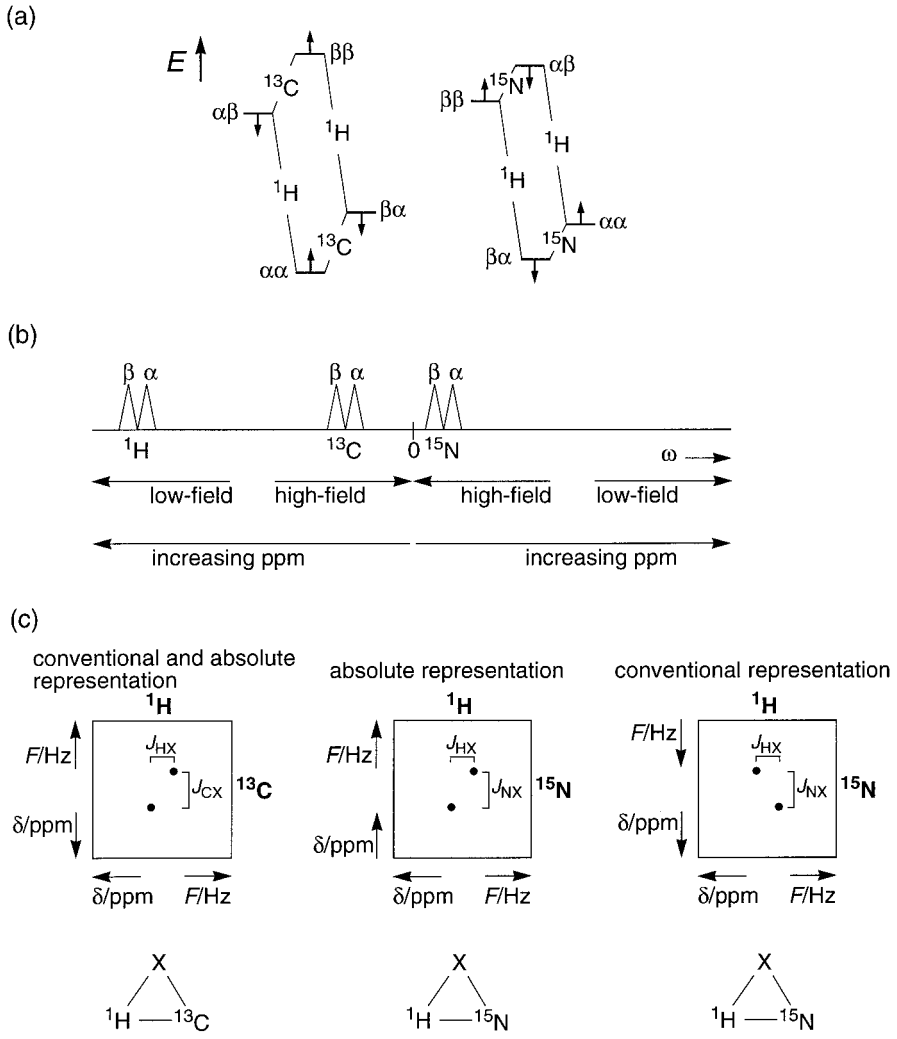

FIG. 5. Energy level diagrams and schematic representations of 1D NMR spectra and 2D cross peaks on absolute and conventional frequency scales. (a) Energy level diagrams of two-spin systems ^{13}C–^{1}H and ^{15}N–^{1}H. The first character on each energy level denotes the spin state of the ^{13}C (^{15}N) spin, the second character that of the X spin. Arrows indicate the way in which the energy levels change for a positive J coupling, i.e., the energy of the spin system is increased when the spin angular momenta are parallel, and is decreased, when the spin angular momenta are opposite (*9*). Note that for the ^{13}C transitions, the energy difference is larger for ^{1}H in spin state β than for ^{1}H in spin state α, whereas for ^{15}N transitions the energy difference is smaller for ^{1}H in spin state β than for ^{1}H in spin state α, leading to the spectral representation shown in (b). (b) 1D NMR spectra of ^{1}H, ^{13}C, and ^{15}N spins on an absolute scale with Larmor frequencies ω increasing from left to right. Note that ^{1}H and ^{13}C NMR spectra are at negative frequencies, as $\omega = -\gamma B_0$ (γ, gyromagnetic ratio; B_0, magnetic field) (*9*). Low-field and high-field spectral regions are indicated separately for spins with positive and negative gyromagnetic ratios. The directions of the respective ppm scales defined by $\delta = (\omega - \omega_{ref})/\omega_{ref}$, where ω_{ref} is the Larmor frequency of a reference compound (e.g., tetramethylsilane), are shown as well. The 1D NMR spectra of the different spins are represented by doublets (not drawn to scale) due to J coupling to a second spin 1/2 (spin X). The labels α and β above the doublet components denote the spin state of spin X if $J > 0$, where the α state has angular momentum $+1/2$ in the direction of the field as in (a). The conventional representation of ^{15}N NMR spectra is the quadrature image of the absolute representation shown here (*9*). (c) Schematic E.COSY-type cross peaks in ^{13}C–^{1}H and ^{15}N–^{1}H correlation spectra. Both spins are assumed to couple with $J > 0$ to a third spin 1/2 (spin X) for which the spin state is unchanged during the pulse sequence. The directions of the ppm scale and the absolute frequency $F = \Omega/2\pi = (\omega - \omega_0)/2\pi$ are indicated with arrows (ω, Larmor frequency; ω_0, carrier frequency). Note that for nuclei with positive gyromagnetic ratio, the sense of the absolute frequency axis F is reversed compared to usual plotting conventions. In the absolute representation of ^{15}N–^{1}H correlation spectra, identical signs of J_{HX} and J_{NX} lead to a positive tilt of the cross peak (the doublet component at high frequencies in both dimensions corresponds to the same state of spin X). The tilt of the cross peak is reversed in the conventional representation of ^{15}N–^{1}H correlation spectra.

difficult than to obtain DQ/ZQ cross peaks correlating the ^{2}J(*trans*) couplings with large intra-TPM J_{HN} couplings in **2** (Table 2, Fig. 3). As a further advantage, DQ/ZQ experiments tend to yield more accurate coupling constant measurements than E.COSY or small flip-angle COSY experiments, when the coupling constants are small compared to the linewidth (*22–24*).

Large time increments can be used with DQ/ZQ experiments, when two different spin types are involved in the mixed

DQ/ZQ coherence, since the carrier frequencies can be set close to the respective nuclei. Large increments make it possible to place relatively long selective inversion pulses in the middle of the evolution time t_1 in order to refocus some of the couplings, simplifying the multiplet fine structure. It also is possible to separate DQ and ZQ cross peaks into different subspectra by appropriate phase cycling which makes it possible to place the carrier at the midpoint of the frequencies of the respective nuclei (*22*, *25*). In the present study, we recorded both cross peaks in a single spectrum with the carrier frequency at the side to avoid any possible confusion about the identity of the DQ and ZQ cross peaks.

All DQ/ZQ experiments presented here are out-and-back experiments; i.e., the coherence transfer pathway reconverting the DQ/ZQ coherence into observable magnetization is a mirror image of the pathway generating the DQ/ZQ coherence from proton magnetization. Although DQ/ZQ experiments could be designed, where the starting spin differs from the spin precessing during the detection period t_2, out-and-back experiments are simpler to design: if the desired coherence can be generated by a particular pulse sequence before the evolution time t_1, the corresponding pulse sequence will also work for the reconversion of the DQ/ZQ coherence into observable magnetization.

As in biomolecular NMR spectroscopy, it is worthwhile to try to generate the DQ/ZQ coherences via coherence transfer pathways which use large coupling constants (*26*). For a strictly linear spin system A–B–C, comparison of the signs of J_{AB} and J_{BC} requires the generation of DQ/ZQ coherence involving the spins A and C. This coherence can be generated either starting from B magnetization by simultaneous evolution under J_{AB} and J_{BC}, or from A (or C) magnetization via a relay through B, sequentially using J_{AB} and J_{BC} (Fig. 4). The DQ/ZQ–HH(N) and DQ/ZQ–HC(N) experiments of Table 2 are examples for the latter case which may represent the most powerful scheme for ^{1}H-detected experiments, when the innermost coordination sphere of the metal ion contains only insensitive nuclei. These features also make DQ/ZQ experiments attractive for the sign determination of residual dipolar couplings of partially oriented macromolecules (*27*).

APPENDIX

Sign Determinations of Coupling Constants from 2D Spectra

By convention, NMR spectra of nuclei with negative (e.g., ^{1}H, ^{31}P, ^{13}C) and positive (e.g., ^{15}N) gyromagnetic ratios are both plotted with ppm scales increasing from right to left. More consistent representations would, however, be obtained if all spectra were plotted on an absolute scale with Larmor frequencies of increasingly positive values to the right. This would correspond to the conventional representation of ^{1}H, ^{31}P, and ^{13}C NMR spectra, but a reversal of ^{15}N NMR spectra (Fig. 5) (*9*).

The evaluation of E.COSY-type cross peak multiplet patterns is simplified by plotting NMR spectra in the absolute representation, i.e., with the ppm scale of ^{15}N NMR spectra reversed compared to the usual representation. For positive J coupling constants, the doublet components corresponding to the α state of a coupled spin 1/2 are always at frequencies more positive than those of the doublet component corresponding to the β state (Fig. 5). In the absolute representation, the tilt of E.COSY-type multiplet patterns in ^{15}N–^{1}H and ^{13}C–^{1}H correlation spectra, resulting from coupling to a third spin X which is not excited during the experiment, can be interpreted without further consideration of the gyromagnetic ratio of the spins involved. Thus, a positive tilt of the ^{15}N–^{1}H cross peak as shown in Fig. 5c would indicate identical signs of J_{HX} and J_{NX} in the same way as a positive tilt of a ^{13}C–^{1}H cross peak indicates identical signs of J_{HX} and J_{CX}. In contrast, a positive tilt in ^{15}N–^{1}H correlation spectra presented in the conventional way indicates opposite signs of J_{HX} and J_{NX}. The conventional representation was used for the experimental spectra of the present publication merely because inversion of the frequency axis is difficult with available software.

The evaluation of DQ/ZQ experiments is also affected by the signs of the gyromagnetic ratios. In the present work, the respective carrier frequencies were always placed at the high-field sides of the ^{1}H, ^{13}C, and ^{15}N resonances involved in the DQ/ZQ coherences. In this way, the double-quantum peak appears at a negative offset larger than that of the zero-quantum peak, if both spins have gyromagnetic ratios of the same sign. For multiple-quantum coherence composed of spins with gyromagnetic ratios of opposite sign, e.g., ^{1}H and ^{15}N, the double-quantum peak appears at an offset smaller than that of the zero-quantum peak, as $F_H = (\omega_H - \omega_{H0})/2\pi < 0$ and $F_N = (\omega_N - \omega_{N0})/2\pi > 0$, and consequently $|F_H + F_N| < |F_H - F_N|$ (ω Larmor frequency, ω_0 carrier frequency).

ACKNOWLEDGMENTS

We thank Dr. Malcolm Levitt for discussions regarding the "sighns" in NMR spectra and a critical reading of the Appendix. Bruker Analytik GmbH, Karlsruhe, is acknowledged for the generous loan of a ^{1}H/^{13}C/^{15}N/^{31}P QXI probehead. G.O. thanks Sydney University for a distinguished visiting scientist scholarship and the Wenner–Gren foundation for a travel grant. L.P.S. acknowledges Sydney University for a H. B. & F. M. Gritton scholarship. B.A.M. thanks the Australian Research Council for financial support. Financial support from the Swedish Natural Science Research Council (Project 10161) is gratefully acknowledged.

REFERENCES

1. D. S. Moore and S. D. Robinson, Hydrido complexes of the transition metals, *Chem. Soc. Rev.* **12,** 415–452 (1983).
2. H. D. Kaesz and R. B. Saillant, Hydride complexes of the transition metals, *Chem. Rev.* **72,** 231–281 (1972).
3. M. V. Baker and L. D. Field, Relative signs of P–P coupling con-

stants in the NMR spectra of octahedral metal phosphine complexes, *Inorg. Chem.* **26,** 2010–2011 (1987).

4. N. Bampos, L. D. Field, and B. A. Messerle, Measurement of heteronuclear coupling constants in organometallic complexes using high-resolution 2D NMR, *Organometallics* **12,** 2529–2535 (1993).
5. P. S. Pregosin and R. W. Kunz, ^{31}P and ^{13}C NMR of transition metal phosphine complexes, *NMR Basic Princ. Prog.* **16,** 1–156 (1979).
6. C. J. Jameson, Spin–spin coupling, *in* "Multinuclear NMR" (J. Mason, Ed.), pp. 89–131, Plenum, New York (1987).
7. F. N. Tebbe, P. Meakin, J. P. Jesson, and E. L. Muetterties, Stereochemically nonrigid six-coordinate hydrides, *J. Am. Chem. Soc.* **92,** 1068–1070 (1970).
8. G. Otting, B. A. Messerle, and L. P. Soler, ^{1}H-detected multinuclear NMR experiments for the measurement of small heteronuclear coupling constants in transition metal complexes, *J. Am. Chem. Soc.* **119,** 5425–5434 (1997).
9. M. H. Levitt, The signs of frequencies and phases in NMR, *J. Magn. Reson.* **126,** 164–182 (1997).
10. G. Otting, B. A. Messerle, and L. P. Soler, ^{1}H-detected, gradient-enhanced ^{15}N and ^{13}C NMR experiments for the measurement of small heteronuclear coupling constants and isotopic shifts, *J. Am. Chem. Soc.* **118,** 5096–5102 (1996).
11. N. Ahmad, J. J. Levison, S. D. Robinson, and M. F. Uttley, Triphenylphosphine complexes of transition metals. Complexes of ruthenium, osmium, rhodium, and iridium containing hydride carbonyl or nitrosyl ligands. *Inorg. Synth.* **15,** 45–64 (1974).
12. L. A. Oro, M. A. Esteruelas, R. M. Claramunt, C. Lopez, J. L. Lavandera, and J. Elguero, Alcohol activation by [Ir(COD)(tris(pyrazol-1-yl)methane]$^{+}$ and [Ir(COD)(tris(pyrazol-1-yl)ethane)]$^{+}$ cations: Formation of alkoxycarbonyl derivatives [(tpzm)IrH(CO_2R')(CO)]$^{+}$ and [(tpze)IrH(CO_2R')(CO)]$^{+}$ (R′ = Me, Et, iPr), *J. Organomet. Chem.* **366,** 245–255 (1989).
13. D. H. Live, D. G. Davis, W. C. Agosta, and D. Cowburn, Long range hydrogen bond mediated effects in peptides: ^{15}N NMR study of gramicidin S in water and organic solvents, *J. Am. Chem. Soc.* **106,** 1939–1941 (1984).
14. T. Berkhoudt and H. J. Jakobsen, Determination of the sign for a one bond ^{15}N–^{15}N spin–spin coupling constant: The flip angle effect, *J. Magn. Reson.* **50,** 323–327 (1982).
15. Y. Kuroda, Y. Fujiwara, and K. Matsushita, Sign determinations and INDO–MO calculations of ^{13}C–^{15}N and ^{15}N–^{15}N spin–spin coupling constants of 3-methyl- and 3,6-dimethyl-pyridazines, *J. Chem. Soc., Perkin Trans.* **2,** 1533–1536 (1985).
16. S. J. Archer, M. Ikura, D. A. Torchia, and A. Bax, An alternative 3D NMR technique for correlating backbone ^{15}N with side chain Hβ resonances in larger proteins, *J. Magn. Reson.* **95,** 636–641 (1991).
17. A. Bax, D. Max, and D. Zax, Measurement of long-range ^{13}C–^{13}C *J* couplings in a 20-kDa protein–peptide complex, *J. Am. Chem. Soc.* **114,** 6923–6925 (1992).
18. A. Bax, G. W. Vuister, S. Grzesiek, F. Delaglio, A. C. Wang, R. Tschudin, and G. Zhu, Measurement of homo- and heteronuclear *J* couplings from quantitative *J* correlation, *Methods Enzymol.* **239,** 79–105 (1994).
19. P. Düx, B. Whitehead, R. Boelens, R. Kaptein, and G. W. Vuister, Measurement of ^{15}N–^{1}H coupling constants in uniformly ^{15}N-labeled proteins: Application to the photoactive yellow protein. *J. Biomol. NMR* **10,** 301–306 (1997).
20. D. Marion, M. Ikura, R. Tschudin, and A. Bax, Rapid recording of 2D NMR spectra without phase cycling. Application to the study of hydrogen exchange in proteins, *J. Magn. Reson.* **85,** 393–399 (1989).
21. G. Otting, A DQ/ZQ NMR experiment for the determination of the signs of small J(^{1}H, ^{13}C) coupling constants in linear spin systems, *J. Magn. Reson.* **124,** 503–505 (1997).
22. A. Rexroth, P. Schmidt, S. Szalma, T. Geppert, H. Schwalbe, and C. Griesinger, New principle for the determination of coupling constants that largely suppress differential relaxation effects, *J. Am. Chem. Soc.* **117,** 10389–10390 (1995).
23. C. Griesinger, O. W. Sørensen, and R. R. Ernst, Correlation of connected transitions by two-dimensional NMR spectroscopy, *J. Chem. Phys.* **64,** 6837–6852 (1986).
24. A. Meissner, T. Schulte-Herbrüggen, and O. W. Sørensen, Relaxation artifacts and their suppression in multidimensional E.COSY-type NMR experiments for measurement of *J* coupling constants in ^{13}C- or ^{15}N-labeled proteins, *J. Am. Chem. Soc.* **120,** 7989–7990 (1998).
25. J. Jarvet and P. Allard, Phase-sensitive two-dimensional heteronuclear zero- and double-quantum-coherence spectroscopy, *J. Magn. Reson. B* **112,** 240–244 (1996).
26. M. Ikura, L. E. Kay, and A. Bax, A novel approach for sequential assignment of ^{1}H, ^{13}C, and ^{15}N spectra of proteins: Heteronuclear triple-resonance three-dimensional NMR spectroscopy. Application to calmodulin, *Biochemistry* **29,** 4659–4667 (1990).
27. N. Tjandra and A. Bax, Direct measurement of distances and angles in biomolecules by NMR in a dilute liquid crystalline medium, *Science* **278,** 1111–1114 (1997).
28. O. W. Sørensen, G. W. Eich, M. H. Levitt, G. Bodenhausen, and R. R. Ernst, Product operator formalism for the description of NMR pulse experiments, *Prog. NMR Spectrosc.* **16,** 163–192 (1983).
29. M. S. Silver, R. I. Joseph, and D. I. Hoult, Highly selective $\pi/2$ and π pulse generation, *J. Magn. Reson.* **59,** 347–351 (1984).
30. M. A. McCoy and L. Mueller, Selective shaped pulse decoupling in NMR: Homonuclear [^{13}C]carbonyl decoupling, *J. Am. Chem. Soc.* **114,** 2108–2112 (1992).
31. G. Bodenhausen and D. J. Ruben, Natural abundance nitrogen-15 NMR by enhanced heteronuclear spectroscopy, *Chem. Phys. Lett.* **69,** 185–189 (1980).
32. G. Otting and K. Wüthrich, Efficient purging scheme for proton-detected heteronuclear two-dimensional NMR, *J. Magn. Reson.* **76,** 569–574 (1988).
33. F. Löhr and H. Rüterjans, Detection of nitrogen–nitrogen *J*-couplings in proteins, *J. Magn. Reson.* **132,** 130–137 (1998).